Two particle correlation effects from rotation and instabilities in heavy ion collisions

Sindre Velle

Department of Physics and Technology, University of Bergen

Master Thesis in Theoretical Physics

May 2013

Abstract

Two particle correlations are studied in the reaction plane of peripheral relativistic heavy ion reactions where the initial state has substantial angular momentum. The earlier predicted rotation effect and Kelvin Helmholtz Instability, leads to space-time momentum correlations among the emitted particles. A specific combination of two particle correlation measurements is proposed, which can sensitively detect the rotation of the emitting system. Here the method is first presented in simple few source models where the symmetries and the possibilities of the detection can be demonstrated in a transparent way. We then look at the method and its result in a high resolution, realistic, computational fluid dynamics model, using the PIC method.

Acknowledgements

Thanks to my advisor László P. Csernai.

Preface

A part of the work presented in the thesis has appeared
in the following publications:

[1] Differential HBT Applied to Relativistic Fluid Dynamics
L.P. Csernai, S. Velle, D.J. Wang, arXiv:1305.0396,
Submitted to Physical Review Letters

[2] Differential HBT Method to Analyze Rotation
L.P. Csernai, S. Velle, arXiv:1305.0385,
Submitted to Journal of High Energy Physics

Contents

Chapter 1

Introduction

Collective flow is one of the most dominant observable features in heavy ion reactions up to the highest available energies, and its global symmetries as well as its fluctuations are extensively studied. Especially at the highest energies for peripheral reaction the angular momentum of the initial state is substantial, which leads to observable rotation according to fluid dynamical estimates [1]. Furthermore the low viscosity quark-gluon fluid may lead to to initial turbulent instabilities, like the Kelvin Helmholtz Instability (KHI), according to numerical fluid dynamical estimates [2], which is also confirmed in a simplified analytic model [3]. These turbulent phenomena further increase the rotation of the system, which also leads to a large vorticity and circulation of the participant zone. [4]. In ref. [2] it is estimated that the increased rotation can be observable via the increased v_1-flow, but the v_1 signal at high energies is weak, so other observables of the rotation are also needed.

The two particle correlation method is used to determine the space-time size of the system emitting the observed particles, thus providing valuable information on the exploding and expanding system at the freeze out stage of a heavy ion collision. This method is based on the Hanbury Brown and Twiss (HBT) method, originally used for the determination of the size of distant stars [5]. In heavy ion collisions the HBT method was used first for the same purpose, the determination of the system size [6], but later also the ellipsoidal shape of the system and its tilt [7, 8]. It was also observed relatively early that the expansion of the system modifies the size estimates due to the collective radial flow velocity of the emitting system [9], while the effect of flow on two particle correlations was also analysed in great detail

[10]. Transport model studies have indicated that the HBT radius shows a minimum at the phase transition threshold [11].

A detailed two particle correlation study of flow rotation was not performed up to now [12]. This became actual now as at higher beam energies, where the initial angular momentum of the participant system is increasing in peripheral reactions, the system may rotate causing a significant and detectable effect.

Different theoretical approaches were worked out up to now to evaluate the two particle correlation functions in different reaction models. We here picked one method, which is not used very frequently up to now, but it can be generalized and used to fluid dynamical models with arbitrary flow patterns well. With this method hereby we study simplified, idealized fluid dynamical systems with different symmetry structures. These studies show how we can detect rotation via two particle correlation functions and what effects may cause difficulties in identifying rotation.

Based on these studies we also present a Differential Hanbury Brown and Twiss (DHBT) method, which can sensitively determine the strength (vorticity or circulation) of the rotating flow and the direction of this rotation.

The Differential HBT method is then used to analyse the fluid dynamical model results of ultra-relativistic heavy ion reactions where the initial state has substantial angular momentum. The rotation effect and Kelvin Helmholtz Instability, leads to space-time momentum correlations among the emitted particles, which can be detected by the method.

We will look at the Differential HBT method and its result in a high resolution, realistic, computational fluid dynamics model, using the PIC method. This model was used to predict the rotation in peripheral ultra-relativistic reactions [1], and to point out the possibility of Kelvin Helmholtz Instability [2]. The model was tested for its numerical viscosity and the resulting entropy production [13], as well as, the vorticity of the flow was analysed in the same model for different configurations [4].

1.1 The Emission Function

Following [14] the definition of a particle 4-current is:

$$N^{\mu} = \int p^{\mu} \frac{d^3p}{p^0} f(x,p) \ , \tag{1.1}$$

where $f(x,p)$ is the invariant scalar phase space density distribution of the emitted particles. The total flow of N nucleons across a space-time (ST) hypersurface, with the surface element, $d\sigma_{\mu}$ is:

$$N = \int \frac{d^3p}{p^0} \int d\sigma_{\mu} \, p^{\mu} f(x,p) \ . \tag{1.2}$$

If we do not perform the integration over the momentum, p, then we get the Cooper-Frye formula [15] for invariant momentum distribution:

$$E\frac{dN}{d^3p} = \int d\sigma_{\mu} \, p^{\mu} f(x,p) \ , \tag{1.3}$$

where $E = p^0$. This assumes that there is a 3-dimensional Freeze Out (FO) hypersurface, which can also be generalized to become a layer, as we will show. Using $d^3\mathbf{p} = dp_{||} d\mathbf{p}_{\perp} = p^0 dy d\mathbf{p}_{\perp}$) we can write this in another form, and we can extend it to a 4-volume integral of a 4-dimensional Source Function, S, as [16, 17]:

$$\frac{dN}{dy d^2p_{\perp}} = \int d\sigma_{\mu}(x) \, p^{\mu} f(x,p) = \int d^4x \, S(x,\mathbf{p}) \ , \tag{1.4}$$

where we assumed that the emission appears on a 3-dimensional hypersurface with the outward pointing normal, $d\sigma^{\mu}$. The emission function gives the distribution of the ST positions of momenta of emitted particles. The emission function gives the number of the particles, ΔN, emitted in the phase-space element $\Delta^3 x \Delta^3 p$ per unit time, Δt. We get a Lorentz invariant scalar if we also multiply it by the energy, p^0, of the emitted particles:

$$S(x,\mathbf{p}) = p^0 \frac{\Delta N}{\Delta t \Delta^3 x \Delta^3 p} \ . \tag{1.5}$$

Along the lines of this introduction we can describe the emission over a hypersurface also as a 4-volume integral. We still assume a ST hypersurface

with an outward pointing normal vector, $d\sigma^\mu$, but then the ST integral is interpreted as a 4-volume integral with a delta function for the given surface, $\delta(x'-x)$ as:

$$\int S(x,\mathbf{p})\, d^4x = \int d^4x\, p^\mu\, \hat{\sigma}_\mu(x')\, \delta^{(4)}(x'-x)\, f(x,p)\ , \tag{1.6}$$

where the emission is constrained to a 3-dimensional hypersurface in the ST and it is directed in a given direction characterized by the unit vector in the source described by $\hat{\sigma}_\mu(x')\,\delta^{(4)}(x')$. Even if we assume that the source is in a ST layer (which is not too thick, e.g. 2-3 fm), in this layer we can have a maximum of the emission. This could even be idealized as a 3-dim hypersurface in the 4-dim ST if the thickness of the layer is neglected. Thus, $\hat{\sigma}_\mu$, is the unit normal vector of this surface:

$$\begin{aligned} \hat{\sigma}^\mu\hat{\sigma}_\mu &= +1 \text{ for timelike hypersurface or layer ,} \\ \hat{\sigma}^\mu\hat{\sigma}_\mu &= -1 \text{ for spacelike hypersurface or layer .} \end{aligned} \tag{1.7}$$

The idealization of FO in a 3D hypersurface is not necessary, however it makes the presentation more transparent. The more realistic emission distribution must happen in a 4D ST surface layer, which can still can have an effective space-like or time-like normal vector. See refs. [10, 18, 19, 20]. Although, one might naively believe that in case of a normal vector, $\hat{\sigma}^\mu = (1,0,0,0)$ the emission is uniform in all spatial directions, this is not true, as the local flow velocity also influences the emission probability [10, 19]. When the flow velocity points in the direction of the detector (or the FO normal) the probability for the emission into the $\hat{\sigma}^\mu$-direction is bigger, so that the emission probability should be proportional to $(u^\mu \cdot \hat{\sigma}_\mu)$. This will be important later on when the observability of rotation is discussed.

In addition even in case of time-like FO the deeper (or earlier) points of the FO layer have a smaller emission probability because of the opacity of QGP, indicated also by the strong jet quenching. This effect causes additional asymmetries in the emission.

1.2 Hydrodynamical Parameterization

Let us assume that at the points of the source the matter is still in local equilibrium. Then we can describe the phase-space distribution of the particles, $f(x,p)$ by a Jüttner distributions [14] or a relativistic Bose-Einstein or Fermi-Dirac distribution. Furthermore, instead of the delta function we may assume the emission distributed in a ST layer, which still has a preferred direction of emission $\hat{\sigma}^\mu$.

For our purposes the most suitable parametrization of the emission function is introduced in the special "Buda-Lund" model, see section 8 of ref. [21] . Here the emission function is parametrized as

$$S(x,\mathbf{p})\, d^4x = p^\mu\, d^4\Sigma_\mu(x)\, f(x,p), \tag{1.8}$$

where the emission probability and its dependence of the FO direction is already included in the $p^\mu\, d^4\Sigma_\mu(x)$ term. The 4-volume integral is directed and yields a maximum for k^μ which is closest to $d^4\Sigma^\mu(x)$. In the Buda-Lund model the FO direction points into the flow 4-velocity, $d^4\Sigma^\mu(x) \propto u^\mu$. This is also a frequent approximation in other fluid dynamical models, although, in the general case it is not a valid approximation. Thus, this approach is identical to the dynamical volume FO in a layer [18, 19, 20], discussed above. We also assume that the FO layer depends parametrically on the proper time, τ, (or distance s^μ)) in the FO factor $d^4\Sigma^\mu(x) \propto \hat{\sigma}^\mu d^4x$. So, that the emission probability is proportional to $G(x)\, H(\tau)$:

$$S(x,\mathbf{p})d^4x = p^\mu\ \hat{\sigma}_\mu(x)\ G(x)\, H(\tau)\ \ d\tau d^3x\ f(x,p)\ ,$$

where

$$H(\tau) = \frac{1}{(2\pi(\Theta)^2)^{1/2}} \exp\left[-\frac{(\tau-\bar{\tau})^2}{2(\Theta)^2}\right], \tag{1.9}$$

and that the width of the emitting sources do not change significantly during the course of emission from a given source.

Then the emission function characterized with a locally thermalized volume-emitting source is:

$$S(x,\mathbf{p})\, d^4x = \frac{g}{(2\pi\hbar)^3} \frac{p^\mu\, \hat{\sigma}_\mu(x)\, G(x)\, H(\tau)\, d\tau d^3x}{\exp\left(\frac{p^\mu u_\mu(x)}{T(x)} - \frac{\mu(x)}{T(x)}\right) - 1}, \tag{1.10}$$

where in place of $f(x,p)$ we inserted the relativistic Bose-Einstein distribution. The factor g stands for the degeneracy, $u^\mu(x)$ is the 4-velocity field, $T(x)$

is the temperature field, $\mu(x)$ is the chemical potential and $d^4x = d\tau\, dx\, dy\, dz$. $G(x)$ is the ST emission density across the layer of the particles (e.g. pions). This can be approximated with a ST hypersurface and then with $\Theta \to 0$ we obtain the Cooper-Frye FO description. [15]

For the phase space distribution we frequently use the Jüttner (relativistic Boltzmann) distribution:

$$f^J(x,p) = \frac{g}{(2\pi\hbar)^3} \exp\left(-\frac{p^\mu u_\mu(x)}{T(x)} + \frac{\mu(x)}{T(x)}\right), \tag{1.11}$$

which is normalized to the invariant scalar density of particles

$$n(x) = N^\mu u_\mu = u_\mu \int \frac{d^3p}{p^0} p^\mu\, f(x,p) = \frac{g e^{\mu/T}}{(2\pi\hbar)^3} C_n, \tag{1.12}$$

where $C_n = 4\pi m^2 T K_2(m/T)$ and we use the $c = k = 1$ convention. Thus in terms of the local invariant scalar particle density the Jüttner distribution is [14]

$$f^J(x,p) = \frac{n(x)}{C_n} \exp\left(-\frac{p^\mu u_\mu(x)}{T(x)}\right). \tag{1.13}$$

We can also define $d\sigma^\mu = dx\, dy\, dz\ \hat{\sigma}^\mu$ (for a timelike surface or layer) where the norm of $d\sigma^\mu$ is the 3-volume of the source element (like a fluid cell), similarly to Refs. [18, 19, 20]

Our source function in this case, Eq. (1.13), similarly to Ref. [21] in the frame where $\hat{\sigma}^\mu = (1,0,0,0)$ is:

$$G(x) = N_{FD}(x)/n(x), \tag{1.14}$$

where $N_{FD}(x)$ is the density of particles arising from fluid-dynamical (FD) evolution (or from other transport models). Then if the flow velocity does not vanish in this frame:

$$N_{FD}(x) = \gamma n(x)\ , \tag{1.15}$$

The $H(\tau)$ (or $H(s)$) freeze-out probability along the τ (or s) parameter, across the layer can be integrated separately from the remaining three orthogonal coordinates.

Here we assume that the primary direction of the emission is $\hat{\sigma}^\mu$. Thus, in case of an explosively expanding system it points towards the detector, so

$\hat{\sigma}^\mu \approx \hat{k}^\mu$. The emission happens from the 4-volume of ST surface layer with an effective normal direction $\hat{\sigma}^\mu$, and not from a ST hypersurface.

In ref. [10] the correlation function was analyzed in detail in dependence of the direction of the primary emission direction, k^μ. A possibility of longitudinal momentum difference was considered in terms of the rapidity of the two emitted particles, where the difference of the longitudinal momenta, the width parameter, was studied in detail. While this analysis provides a deeper insight into the features of the correlation function, in our studies we concentrate to the rotation of the system and restrict ourself to a simplest presentation of the correlation function, which can be realized experimentally without much additional effort.

We can assume FO from a narrow layer at a proper time hyperbola $\tau_{FO} = cons.$ like in the Buda-Lund model, see ref. [21]. This can be practical if the CFD model uses proper time and rapidity coordinates. Recent studies indicate that irrespective of the coordinate system choice, in the major part of FO in high energy collisions the FO happens near to a constant proper time hyperbola, although the origin of this FO-hyperbola is at an earlier point of time than the intersection of the centers of the projectile and target trajectories [22].

For the first test purpose we take an oversimplified model of 4 fluid elements, which may or may not expand or rotate. We assume that these are in the reaction plane, $[x-z]$-plane, and will characterise parameters of a heavy ion reaction based on CFD results. We assume that the system is stationary so the time emission probability is a Gaussian (like) distribution in time. Later on we intend to study and see that these methods can be applied for realistic full scale FD calculations also.

1.3 Pion Correlation Functions

The pion correlation function is defined as the inclusive two-particle distribution divided by the product of the inclusive one-particle distributions, such that [17]:

$$C(p_1, p_2) = \frac{P_2(p_1, p_2)}{P_1(p_1) P_1(p_2)}, \tag{1.16}$$

where p_1 and p_2 are the 4-momenta of the pions.

We will assume pions are created at two points, x_1 and x_2, which are distributed in space. The particle distribution is given by the reduced phase

space source distribution:

$$S(x,p) = f(x,p)\, p^{\mu}\, \hat{\sigma}_{\mu}\, G(x)\, H(\tau)\ . \tag{1.17}$$

For two identical pions with momenta p_1 and p_2 the two-particle distribution is:

$$P_2(p_1,p_2) = \int d^4x_1 d^4x_2\, S(x_1,p_1) S(x_2,p_2) |\psi_{12}|^2, \tag{1.18}$$

where the wave equation ψ_{12} is given by:

$$\psi_{12} = \frac{1}{\sqrt{2}}(e^{ip_1\cdot x_1 + ip_2\cdot x_2} + e^{ip_1\cdot x_2 + ip_2\cdot x_1}) \tag{1.19}$$

We now introduce the center-of-mass momentum [1]

$$k = \frac{1}{2}(p_1 + p_2), \tag{1.20}$$

and the relative momentum

$$q = p_1 - p_2, \tag{1.21}$$

where assuming the mass-shell constraint for the two particles and so we have $q\cdot k = (p_1 - p_2)\cdot(p_1 + p_2)/2 = (p_1^2 - p_2^2)/2 = (m_\pi^2 - m_\pi^2)/2 = 0$, which leads to $q^0 = \mathbf{q}\cdot\mathbf{k}/k^0$

With the relative and center-of-mass momentum we can write the wave equation as:

$$\psi_{12} = \frac{e^{ik\cdot(x_1+x_2)}}{\sqrt{2}} \left(e^{iq\cdot(x_1-x_2)/2} + e^{-iq\cdot(x_1-x_2)/2}\right)\ , \tag{1.22}$$

and then

$$|\psi_{12}|^2 = \left[1 + \frac{1}{2}\left(e^{iq\cdot(x_1-x_2)} + e^{-iq\cdot(x_1-x_2)}\right)\right]\ . \tag{1.23}$$

We can then insert eq. (1.23) into eq. (1.18), and we obtain:

$$\begin{aligned} P_2(p_1,p_2) &= \int d^4x_1\, d^4x_2\, S(x_1, k+q/2)\, S(x_2, k-q/2) \\ &\times \left[1 + \frac{1}{2}\left(e^{iq\cdot(x_1-x_2)} + e^{-iq\cdot(x_1-x_2)}\right)\right]\ , \end{aligned} \tag{1.24}$$

[1] The vector $\mathbf{k}$ is the wavenumber vector, $\mathbf{k} = \mathbf{p}/\hbar$ so for numerical calculations we have to use that $\hbar c = 197.327$ MeV fm., The same applies to $\mathbf{q}$.

where the last term in the brackets is $\cos[q(x_1 - x_2)]$. Similarly for the one particle distribution we get:

$$P_1(p) = \int d^4x \; S(x,k) \; . \tag{1.25}$$

We now use a method for moving sources presented in ref. [23]. Using eqs. (1.24,1.25), together with the definition of the correlation function we have:

$$C(k,q) = 1 + \frac{R(k,q)}{\left|\int d^4x \, S(x,k)\right|^2} \; , \tag{1.26}$$

where

$$R(k,q) = \int d^4x_1 \, d^4x_2 \; \cos[q(x_1 - x_2)] S(x_1, k + q/2) \, S(x_2, k - q/2) \; . \tag{1.27}$$

Here $R(k,q)$ can be calculated [23] via the function

$$\begin{aligned} J(k,q) = \int d^4x \; S(x, k + q/2) \; \exp(iqx) = \\ \int d^4x \; S(x, k + q/2) \, [\cos(qx) + i \sin(qx)] \; , \end{aligned} \tag{1.28}$$

and we obtain the $R(k,q)$ function as

$$R(k,q) = \mathrm{Re}\, [J(k,q) \, J(k,-q)] \tag{1.29}$$

This can be verified, by using eq. (1.28), forming a double integral over $d^4x_1 \, d^4x_2$ from $J(k,q) \, J(k,-q)$, yielding to a term $\exp[-iq(x_1 - x_2)]$. Then taking the real part of the double integral leads to a term $\cos[q(x_1 - x_2)]$ and this recovers eq. (1.27).

1.3.1 Source with local Jütner distribution

Let us take the $S(x_1,p_1)S(x_2,p_2)$ term in eq. (1.24), and assume that the single particle distributions, $f(x,p)$, in the source functions are Jüttner distributions, which depend on the local velocity, $u^\mu(x)$, via the term

$$\exp\left(\frac{-p^\mu u_\mu(x)}{T(x)}\right) \tag{1.30}$$

as shown in eq. (1.13). Here the local flow velocity may be different in different locations, x_1 and x_2, and this influences the correlations of the observed momenta. Thus, the scalar products in terms of k and q become:

$$\begin{aligned} &\exp(-p_1 u_1)\, \exp(-p_2 u_2) = \\ &\exp(-(k+q/2)\, u_1)\, \exp(-(k-q/2)\, u_2) = \\ &\exp(-k u_1)\, \exp(-k u_2)\, \exp(-q(u_1-u_2)/2) \end{aligned} \tag{1.31}$$

where we used the notation $u_1 = u(x_1) = u^\mu(x_1)$. We assume that for a given detector position the normal direction of the emission is approximately the same, so for the two sources the term $p^\mu \hat{\sigma}_\mu(x)$ is the same and it cancels in the nominator and denominator.

Thus, the expression of the correlation function, eq. (1.27) will be modified to

$$\begin{aligned} R(k,q) = \int d^4x_1 d^4x_2\, S(x_1,k) S(x_2,k) \cos[q(x_1-x_2)] \times \\ \exp\left[-\frac{q}{2}\left(\frac{u(x_1)}{T(x_1)} - \frac{u(x_2)}{T(x_2)}\right)\right], \end{aligned} \tag{1.32}$$

and the corresponding $J(k,q)$ function will become

$$J(k,q) = \int d^4x\; S(x,k)\, \exp\left[-\frac{q}{2}\frac{u(x)}{T(x)}\right]\, \exp(iqx)\;, \tag{1.33}$$

In eq. (1.32) the term including the momentum component q and the flow velocity u becomes unity if the source has a uniform distribution of $u(x)/T(x)$, and in this case we may be able to use the so called *smoothness approximation*: $S(x,k+q/2)S(y,k-q/2) \approx S(x,k)S(y,k)$, and the correlation function, expression (1.26), takes the form

$$C(k,q) = 1 + \frac{\left|\int d^4x\; e^{iqx} S(x,k)\right|^2}{\left|\int d^4x\, S(x,k)\right|^2}\;, \tag{1.34}$$

Chapter 2

Symmetric Few Source Models

2.1 One Fluid Cell as Source

We now assume a source function, which is reduced to one Freeze Out (FO) time moment. Thus the integration over the 4-volume of an emission layer is reduced to the 3-volume of a FO hypersurface. For simplicity, we assume FO at a constant coordinate time t, where we assume a local Jüttner distribution. Thus, we have the source function as

$$S(x,k) = G(x)\, H(\tau) \exp\left(-\frac{k_\mu u^\mu(x)}{T(x)}\right) k^\mu\, \hat{\sigma}_\mu \ , \tag{2.1}$$

where $k^\mu \hat{\sigma}_\mu$ is an invariant scalar, and for a single cell we use a simple quadratic parametrization for $n(x)$ as:

$$G(x) = \gamma n(x) = \gamma n_s \exp\left(-\frac{x^2+y^2+z^2}{2R^2}\right). \tag{2.2}$$

Here n_s is the average density of the Gaussian source (or fluid cell) of mean radius R.

2.1.1 Steady source

Let us start with a single source at rest. The invariant scalar $k^\mu u_\mu$ can be calculated in the frame where the cell is at rest. We have then

$$u^\mu = (1,0,0,0) \Rightarrow -\frac{k_\mu u^\mu}{T} = -\frac{k^0}{T} = -\frac{E_k}{T} \ , \tag{2.3}$$

In this simplest case we also assume that the FO direction is $\hat{\sigma}^\mu = (1,0,0,0)$, so the τ-coordinate coincides with the t-coordinate, and it is orthogonal to the $x, y, x-$ coordinates. Then we can make use of the following integral:

$$\int_{-\infty}^{+\infty} e^{-ax^2} d^3x = \left(\frac{\sqrt{\pi}}{\sqrt{a}}\right)^3 , \tag{2.4}$$

We can perform the integral along the t direction of $H(t)$, which gives unity and then the single particle distribution is

$$\begin{aligned} &\int d^4x\ S(x,k) = \frac{n_s}{C_n}\ (k^\mu \hat{\sigma}_\mu)\ \exp\left(-\frac{E_k}{T_s}\right) \times \\ &\int_{-\infty}^{+\infty} H(t)dt \int_{-\infty}^{+\infty} e^{-\frac{x^2}{2R^2}} dx \int_{-\infty}^{+\infty} e^{-\frac{y^2}{2R^2}} dy \int_{-\infty}^{+\infty} e^{-\frac{z^2}{2R^2}} dz\ = \\ &n_s\ (k^\mu \hat{\sigma}_\mu)\ \exp\left(-\frac{E_k}{T_s}\right) \frac{(2\pi R^2)^{3/2}}{C_n}\ , \end{aligned} \tag{2.5}$$

where T_s is the temperature of the source, and $E_k = k^0$ in the rest frame of the fluid cell. Due to the normalization of $H(t)$ the integral over the time t is unity. The contribution to the nominator from Eq. (1.33) is

$$\begin{aligned} &J(k,q) = \int d^4x\, e^{iq\cdot x} e^{-q^0/(2T_s)} S(x,k)\ =\ \frac{n_s\,(k^\mu \hat{\sigma}_\mu)}{C_n}\ \times \\ &\exp\left[-\frac{E_k + q^0/2}{T_s}\right] \int_{-\infty}^{+\infty} H(t) e^{iq^0 t} dt \int_{-\infty}^{+\infty} e^{-\frac{x^2}{2R^2}} e^{-iq_x x} dx\ \times \\ &\int_{-\infty}^{+\infty} e^{-\frac{y^2}{2R^2}} e^{-iq_y y} dy \int_{-\infty}^{+\infty} e^{-\frac{z^2}{2R^2}} e^{-iq_z z} dz = \\ &\frac{n_s(k^\mu \hat{\sigma}_\mu)}{C_n} \left(2\pi R^2\right)^{3/2} \exp\left[-\frac{E_k}{T_s}\right] \exp\left[-\frac{q^0}{2T_s}\right] \times \\ &\exp\left[-\frac{R^2}{2} q^2\right] \exp\left[-\frac{\Theta^2}{2} (\hat{\sigma}^\mu q_\mu)^2\right], \end{aligned} \tag{2.6}$$

where we used $\int_{-\infty}^{\infty} \exp(-p^2x^2 \pm qx)dx = (\sqrt{\pi}/p) \times \exp(q^2/(4p^2))$ [24] 3.323/2. In the time integral the present choice of $\hat{\sigma}^\mu$ would give $(q^0)^2$, but we wanted to indicate that other choices are also possible and they would yield $(\hat{\sigma}^\mu q_\mu)^2$. In the $J(k,q)J(k,-q)$ product the terms $\exp[\pm q^0/(2T_s)]$ cancel each other. Inserting these equations into (1.26) we get

$$C(k,q) = 1 + \exp\left(-(\Theta)^2 (\hat{\sigma}^\mu q_\mu)^2 - R^2 q^2\right)\ . \tag{2.7}$$

If we have a source at a point in the FO layer, which is at a longer distance from the external side of the FO layer than Θ, then the contribution of the time integral from this point is reduced. In a few source model it is more transparent to describe this reduction by assigning a smaller weight factor to the contribution of the deeper lying source.

If we tend to an infinitely narrow FO layer, $\Theta \to 0$, i.e. to a FO hypersurface, then

$$C(k,q) = 1 + \exp\left(-R^2 q^2\right) \ . \tag{2.8}$$

The k dependence thus drops out from the correlation function, $C(k,q)$ as the k dependent parts are separable. See Fig. 2.1. The size of the fluid cells in a high resolution 3+1D fluid dynamical calculation is $(0.3\text{fm})^3$. With this resolution the *numerical viscosity* of the fluid dynamcal calculation [13] is the same as the estimated minimal viscosity of the QGP [25] which occurs at the critical point of the phase transition [26]. As Fig. 2.1 shows the correlation for such a cell size yields to an extended distribution in the relative momentum q.

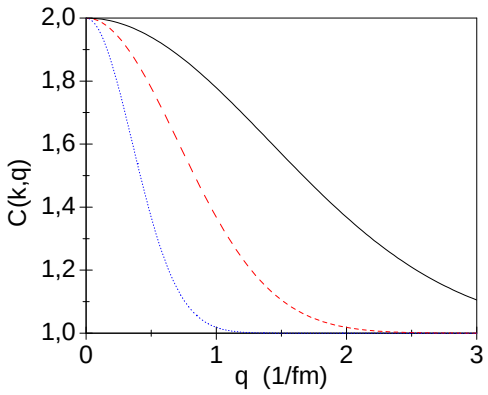

Figure 2.1: (color online) The correlation function, $C(k,q)$, for a single, static, spherically symmetric, Gaussian source with different radii, $R = 4, 1$ and 0.25 fm, (blue-dotted, red-dashed, and full-black lines respectively), as described by eq. (2.8).

For the study of the rotation of the system the thickness of the FO layer is of secondary importance, especially if we discuss only a few fluid sources. In this case the role of the depth of a source point within the layer is given by its reduced contribution to the particle emission. This can be represented

much simpler with assigning emission weights to the small number of sources. Thus, in the following discussion, we do not go into the details of the time structure of the emission.

2.1.2 Moving source

Now for a moving source in the x-direction with a velocity v_x we have, $u_s^\mu = \gamma_s(1, v_x, 0, 0)$ the scalar product $k \cdot u_s/T_s = k_\mu u_s^\mu/T_s$ provides an additional contribution to the correlation function. However, in the case of a single fluid cell or a single source the velocity and the temperature do not change within the cell, so the modifying term in eq. (1.32) becomes unity. We use $k_\mu u^\mu = \gamma(E_k - k_x v_x)$, and the source function becomes

$$S(x,k) = \frac{n(x)\,(k^\mu\,\hat{\sigma}_\mu)}{C_n}\,\exp\left[-\frac{k\cdot u_s}{T_s}\right]\,, \tag{2.9}$$

where $[k \cdot u_s/T_s] = [\gamma_s(E_k - k_x v_x)/T_s]$.

Within the source (or fluid element) the velocity u_s and temperature T_s are assumed to be the same. The source of fluid element may have a density profile, but this profile should be the same for all cells (although the average density, n_s is not the same for all cells. The spatial integrals can be performed in the rest frame of the cell, giving the same integral result as above (2.5), because the moving cellsize shrinks, but the apparent density increases, so that the total number of particles in a cell remains the same as it is an invariant scalar. Then the integral of the single particle contribution is

$$\begin{aligned} J(k,q) &= \int d^3x\, e^{iq\cdot x} S(x,k) \exp\left[-\frac{q\cdot u_s}{2T_s}\right] \\ &= n_s(k^\mu\hat{\sigma}_\mu)\exp\left[-\frac{k\cdot u_s}{T_s}\right]\,\frac{(2\pi R^2)^{3/2}}{C_n}\,. \end{aligned} \tag{2.10}$$

Then the two particle distribution:

$$\begin{aligned} &J(k,q) = \int d^3x\, e^{iq\cdot x} S(x,k) \exp\left[-\frac{q\cdot u_s}{2T_s}\right] = \\ &n_s(k^\mu\hat{\sigma}_\mu)\exp\left[-\frac{k\cdot u_s}{T_s}\right]\exp\left[-\frac{q}{2}\frac{u_s}{T_s}\right]\,\frac{(2\pi R^2)^{3/2}}{C_n}\exp\left(-\frac{R^2}{2}q^2\right)\,. \end{aligned} \tag{2.11}$$

When calculating $R(k,q)$, in the $J(k,q)J(k,-q)$ product the terms $\exp[\pm q\cdot u_s/(2T_s)]$ cancel each other. In the formulae the $\hbar = 1$ convention is used and k and q are considered as the wavenumber vectors.

We then insert these equations into equation (1.26) and we get for one moving Gaussian source

$$C(k,q) = 1 + \exp\left(-R^2q^2\right) \ . \tag{2.12}$$

Again, this result does not depend on k, just as the previous single source at rest, eq. (2.8).

2.2 Two Fluid Cell Sources

2.2.1 Two steady sources

For emission from two steady sources, two particle correlations were studied in ref. [21]. Here we use the present method. We assume that the two source system is symmetric both their positions are placed symmetrically and also their FO normal vectors, $\hat{\sigma}^\mu$, are the same. If the normal $\hat{\sigma}^\mu$ were $(1,0,0,0)$, then the invariant scalar $k^\mu\hat{\sigma}_\mu$ would be $k^0 = E_k$, although we do not need this additional requirement to illustrate the correlation function, which would arise from an idealized symmetric system.

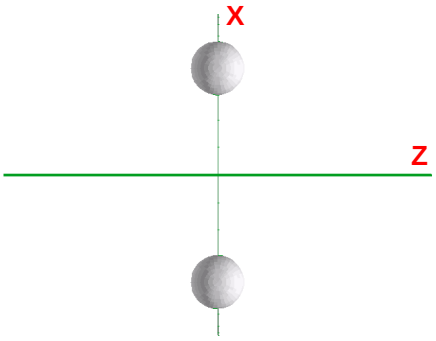

Figure 2.2: (color online) Two steady sources in the reaction ($[x-z]$) plane with a distance between them of $2d$ in the $x-$direction.

We also assume that the time distributions, $H(\tau)$ for the two sources are identical, so these can be integrated simultaneously and yield unity. If we have two sources then the source function is

$$S(x,k) = \sum_s S_s(x,k) = (k^\mu \hat{\sigma}_\mu) \sum_s \frac{n_s(x)}{C_{ns}} \exp\left[-\frac{k\cdot u_s}{T_s}\right] , \tag{2.13}$$

while the J function in the Jüttner approximation is

$$J(k,q) = \sum_s \exp\left[-\frac{q}{2}\frac{u_s}{T_s}\right] \exp(iqx_s) \int_S d^4x \; S_s(x,k) \exp(iqx) , \tag{2.14}$$

where x_s is the position of the center of the source, and the spatial integrals run separately for each of the identical sources, i.e. we assume fluid cells with identical density profiles, but with different densities, n_s and temperatures, T_s.

In case of steady sources $u_s = (1,0,0,0)$, and the spatial integral for one source is the same as for a single source. Thus,

$$\begin{aligned} \int d^3x \; S(x,k) = \sum_s \int_S d^3x \; S_s(x,k) = \\ \left(2\pi R^2\right)^{3/2} (k^\mu \hat{\sigma}_\mu) \sum_s \frac{n_s}{C_{ns}} \exp\left(-\frac{E_k}{T_s}\right) \end{aligned} \tag{2.15}$$

and

$$\begin{aligned} J(k,q) = \sum_s \exp\left[-\frac{q^0}{2T_s}\right] \exp(iqx_s) \int_S d^3x \; S_s(x,k) \exp(iqx) = \\ \left(2\pi R^2\right)^{3/2} \; (k^\mu \hat{\sigma}_\mu) \; \exp\left(-\frac{R^2}{2}q^2\right) \; \sum_s \frac{n_s}{C_{ns}} \; \times \\ \exp\left(-\frac{E_k}{T_s}\right) \exp\left[-\frac{q^0}{2T_s}\right] \exp(iq^0 x_s^0) \exp(-i\mathbf{q}\mathbf{x}_s) \; . \end{aligned} \tag{2.16}$$

In the $J(k,q)J(k,-q)$ product the terms $\exp[\pm q^0/(2T_s)]$ cancel each other. Both $J(k,q)$ and $J(k,-q)$ includes a sum $[\exp(i\mathbf{q}\mathbf{x}_s)+\exp(-i\mathbf{q}\mathbf{x}_s)]$, and their product leads to a factor $2[1+\cos(2\mathbf{q}\mathbf{x}_s)]$. Here we assumed that the time-like extent of the emission layer is negligible compared to the space-like size. Consequently, if the two sources have the same parameters, just different locations, $x_1 = -x_2$ (see Fig. 2.2) then

$$C(k,q) = 1 + \frac{1}{2}\exp(-R^2q^2)[1+\cos(2\mathbf{q}\mathbf{x}_s)] \tag{2.17}$$

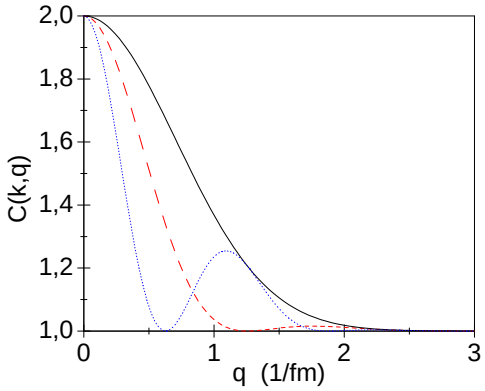

Figure 2.3: (color online) The correlation function, $C(k,q)$, for two spherical, Gaussian sources at rest, shown in the direction of the displacement (here q_x) with different distances, $d = 2.5, 1.25$ and 0 fm, (dotted-blue, dashed-red, and full-black lines respectively) and in the orthogonal direction, q_y which is identical with the $d = 0$ contribution (full-black line). For finite d the cosine term results in a modification in the direction of the line joining the sources, which becomes apparent if the distance between the sources becomes small compared to the size of the spherical sources.

This result agrees with ref. [21], section 9.1 (p. 41), and in the limit of $\mathbf{x}_s = 0$ it returns the single source result, eq. (2.8). See Fig. 2.3. If the distance of the two sources is $2d$, i.e. $x_1 = d$ and $x_2 = -d$, then $2\mathbf{q}\mathbf{x}_s = 2q_x\, d$, thus the modification appears in the q_x-direction only. In the other directions, q_y and q_z, the single source result (2.8) is returned.

If the distance of the two sources, $2d$, is comparable or smaller than the radius of a single source, R, then the two source configuration leads to visible zero points, $C(k,q) = 0$, on the q_x-axis at $2q_x\, d = \pm(1+2n)\pi$, where $n = 0, 1, 2, 3, \ldots$. In Fig. 2.3 for the $d = 2.5$fm case we see these zero points at $q_x = \pi/(2d), 3\pi/(2d)\,,\ \ldots$, while at the points $q_x = 2\pi/(2d), 4\pi/(2d)\,,\ \ldots$ the distribution function, $C(k,q_x)$ touches (becomes tangent to) the distribution function for $d = 0$ or the distribution function $C(k,q_y)$.

The appearance of the zero points is to a large extent an artifact of the used very simplistic two source model. In case of other additional sources these zero points would disappear. Nevertheless, this feature illustrates that the correlation function can be more complex than a set of Gaussians of the momentum difference q in different directions or at different rapidities.

2.2.2 Two moving sources

For two moving sources, the same way as before but where the two sources are moving in opposite directions, so $u_s = u_1$ or u_2 where $u_1^\mu = (\gamma_s, \gamma_s \mathbf{v}_1)$, $u_2 = \bar{u}_s^\mu = (\gamma_s, \gamma_s(-\mathbf{v}_1))$, and $\mathbf{u}_s \equiv \gamma_s \mathbf{v}_s$, so that $\mathbf{u}_1 = -\mathbf{u}_2$. Similarly, $x_s = x_1$ or x_2 where $x_s^\mu = (t_s, \mathbf{x}_s)$, $\bar{x}_s^\mu = (t_s, -\mathbf{x}_s)$, and $\mathbf{x}_1 = -\mathbf{x}_2$. For now we also assume that FO happens at a t =const. FO hypersurface, so $d\hat{\sigma}^\mu = (1, 0, 0, 0)$ and so $t_1 = t_2$.

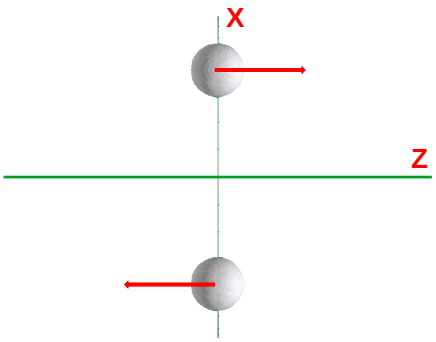

Figure 2.4: (color online) Two moving sources in the reaction ($[x-z]$) plane with a distance between them of $2d$ in the $x-$direction. The sources are moving in the directions indicated by the (red) arrows.

If we have several sources then the source function in Jüttner approximation is

$$S(x,k) = \sum_s S_s(x,k) = (k^\mu \, \hat{\sigma}_\mu) \, \sum_s \frac{n_s(x)}{C_{ns}} \, \exp\left[-\frac{k \cdot u_s}{T_s}\right] \, , \tag{2.18}$$

while the J function is

$$J(k,q) = \sum_s \exp\left[-\frac{q}{2}\frac{u_s}{T_s}\right] \exp(iqx_s) \int_S d^4x \; S_s(x,k) \, \exp(iqx) \, , \tag{2.19}$$

where x_s is the 4-position of the center of source s, and the spatial integrals run separately for each of the identical sources, i.e. we assume fluid

cells with identical density profiles, but with different densities, n_s, velocities, u_s and temperatures, T_s.

The spatial integral for one source is the same as for a single source. Thus,

$$\int d^3x\ S(x,k) = \sum_s \int_S d^3x\ S_s(x,k) =$$
$$(k^\mu\,\hat{\sigma}_\mu)\ \left(2\pi R^2\right)^{3/2}\ \frac{n_s}{C_{ns}} \exp\left(-\frac{k^0\gamma_s}{T_s}\right)\left[\exp\left(\frac{\mathbf{k}\mathbf{u}_s}{T_s}\right) + \exp\left(-\frac{\mathbf{k}\mathbf{u}_s}{T_s}\right)\right]\ . \tag{2.20}$$

This returns eq. (2.15) if $u_s = (1,0,0,0)$. The function $J(k,q)$ becomes

$$J(k,q) = \sum_s \exp\left[-\frac{q\cdot u_s}{2T_s}\right]\ \exp(iqx_s)\int_S d^4x\ S_s(x,k)\ \exp(iqx) =$$
$$(k^\mu\,\hat{\sigma}_\mu)\ \left(2\pi R^2\right)^{3/2} \exp\left(-\frac{R^2q^2}{2}\right)\sum_s \frac{n_s}{C_{ns}} \exp\left[-\frac{k\cdot u_s}{T_s}\right]\exp\left[-\frac{q\cdot u_s}{2T_s}\right]\ \exp(iqx_s) =$$
$$(k^\mu\,\hat{\sigma}_\mu)\ \left(2\pi R^2\right)^{3/2} \exp\left(-\frac{R^2}{2}q^2\right)\frac{n_s}{C_{ns}} \exp\left[-\frac{k^0\gamma_s}{T_s}\right]\exp\left[-\frac{q^0}{2}\frac{\gamma_s}{T_s}\right]\exp(iq^0x_s^0)\times$$
$$\left[\exp\left[\frac{\mathbf{k}\mathbf{u}_s}{T_s}\right]\exp\left[\frac{\mathbf{q}\mathbf{u}_s}{2T_s}\right]\exp(-i\mathbf{q}\mathbf{x}_s) + \exp\left[-\frac{\mathbf{k}\mathbf{u}_s}{T_s}\right]\exp\left[-\frac{\mathbf{q}\mathbf{u}_s}{2T_s}\right]\exp(i\mathbf{q}\mathbf{x}_s)\right], \tag{2.21}$$

where the factor $\exp(iq^0x_s^0)$ can be dropped if the FO time distribution is simultaneous for the two sources, because then $x_s^0 = 0$. This returns eq. (2.16) if $u_s = (1,0,0,0)$.

Now we can divide the two particle correlation with the square of the single particle distribution

$$\begin{aligned}
\frac{Re\left[J(k,q)\,J(k,-q)\right]}{\left|\int d^4x\, S(x,k)\right|^2} &= \exp(-R^2q^2)\frac{Re\left[e^{\frac{2\mathbf{ku}_s}{T_s}}+e^{-\frac{2\mathbf{ku}_s}{T_s}}+e^{\frac{\mathbf{qu}_s}{T_s}}e^{i2\mathbf{qx}_s}+e^{-\frac{\mathbf{qu}_s}{T_s}}e^{-i2\mathbf{qx}_s}\right]}{\left(e^{\frac{\mathbf{ku}_s}{T_s}}+e^{-\frac{\mathbf{ku}_s}{T_s}}\right)^2} \\
&= \exp(-R^2q^2)\times \\
&\frac{Re\left[2\cosh\left(\frac{2\mathbf{ku}_s}{T_s}\right)+e^{\frac{\mathbf{qu}_s}{T_s}}\left(\cos(2\mathbf{qx}_s)+i\sin(2\mathbf{qx}_s)\right)+e^{-\frac{\mathbf{qu}_s}{T_s}}\left(\cos(-2\mathbf{qx}_s)+i\sin(-2\mathbf{qx}_s)\right)\right]}{2\left[\cosh\left(\frac{2\mathbf{ku}_s}{T_s}\right)+1\right]} \\
&= \exp(-R^2q^2)\frac{\cosh\left(\frac{2\mathbf{ku}_s}{T_s}\right)+\cosh\left(\frac{\mathbf{qu}_s}{T_s}\right)\cos(2\mathbf{qx}_s)}{\cosh\left(\frac{2\mathbf{ku}_s}{T_s}\right)+1}
\end{aligned} \tag{2.22}$$

Consequently, if the two sources have the same parameters, just opposite locations with respect to the center, and opposite velocities, then the correlation function is

$$C(k,q) = 1+\exp(-R^2q^2)\,\frac{\cosh\left(\frac{2\mathbf{ku}_s}{T_s}\right)+\cosh\left(\frac{\mathbf{qu}_s}{T_s}\right)\cos(2\mathbf{qx}_s)}{\cosh\left(\frac{2\mathbf{ku}_s}{T_s}\right)+1}\,. \tag{2.23}$$

This returns eq. (2.17) if $u_s=(1,0,0,0)$, and $C(k,q)=2$ if $q=0$.

If we have two sources placed at $x=\pm d_x$, and with the velocity in the $\pm z$-direction, $\pm v_z$, then the correlation function is for the different directions becomes:

$$\begin{aligned}
C(k_x,q_x) &= 1+\frac{1}{2}\exp(-R^2q_x^2)\left[1+\cos\left(2q_xd_x\right)\right]\,, \\
C(k_x,q_y) &= 1+\exp(-R^2q_y^2)\,, \\
C(k_x,q_z) &= 1+\frac{\exp(-R^2q_z^2)}{2}\left[1+\cosh\left(\frac{\gamma q_z v_z}{T_s}\right)\right]\,.
\end{aligned} \tag{2.24}$$

$$
\begin{aligned}
C(k_y, q_x) &= 1 + \frac{1}{2}\exp(-R^2 q_x^2)\left[1 + \cos\left(2q_x d_x\right)\right] \ , \\
C(k_y, q_y) &= 1 + \exp(-R^2 q_y^2) \ , \\
C(k_y, q_z) &= 1 + \frac{\exp(-R^2 q_z^2)}{2}\left[1 + \cosh\left(\frac{\gamma q_z v_z}{T_s}\right)\right] \ .
\end{aligned}
\tag{2.25}
$$

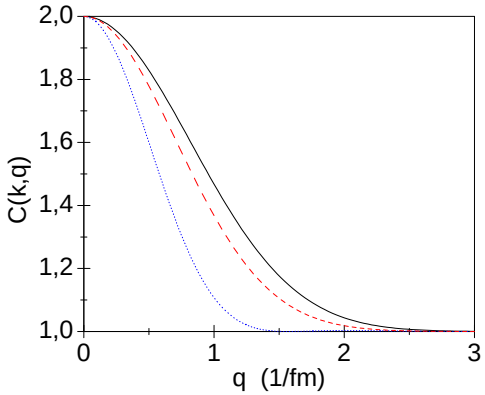

Figure 2.5: (color online) The correlation functions, $C(k, q)$, for two moving sources where the displacement of the sources is in the x-direction, and the center-of-mass momentum, $\mathbf{k}$, of emitted particles is in the x and y direction. The solid black line is for the momentum difference, q_z, the dashed red line is for q_y and dotted blue line is for q_x. The radius of the sources is $R = 1$fm, (same as in Fig. 2.3), the displacement is $d = 1$fm, and the source velocity is, $\gamma v_z/T_s = 1.0$ fm. This can be satisfied e.g. by $u_s = 0.6$c and $T = 0.12$GeV.

$$
\begin{aligned}
C(k_z, q_x) &= 1 + \exp(-R^2 q_x^2)\,\frac{\cosh\left(\frac{2\gamma k_z v_z}{T_s}\right) + \cos\left(2q_x d_x\right)}{\cosh\left(\frac{2\gamma k_z v_z}{T_s}\right) + 1} \ , \\
C(k_z, q_y) &= 1 + \exp(-R^2 q_y^2) \ , \\
C(k_z, q_z) &= 1 + \exp(-R^2 q_z^2)\,\frac{\cosh\left(\frac{2\gamma k_z v_z}{T_s}\right) + \cosh\left(\frac{\gamma q_z v_z}{T_s}\right)}{\cosh\left(\frac{2\gamma k_z v_z}{T_s}\right) + 1} \ .
\end{aligned}
\tag{2.26}
$$

Therefore only the correlation functions in the k_z, q_x-direction and in the q_z-directions are affected by the z-directed velocity of the source. In this

direction, k_z, unfortunately it is difficult to detect the two particle correlations. For the k_x and k_y-directions the q_x-distribution is affected by the displacement of the two sources by $\pm d_x$. The q_y-distribution is not effected by either the displacement or the source velocities.

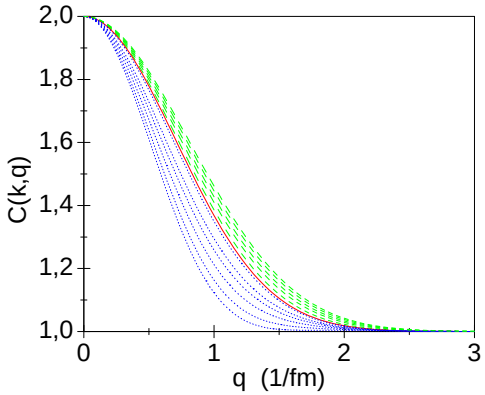

Figure 2.6: (color online) The correlation functions, $C(k, q)$ for two moving sources where the displacement of the sources is in the x-direction, and the center-of-mass momentum, $\mathbf{k}$, of emitted particles is in the x-direction. The dashed green lines are for the relative momentum, q_x, the solid red line is for q_y and dotted blue lines are for q_z. For large values of the center-of-mass momentum k_x the correlation functions $C(k_x, q_x)$ and $C(k_x, q_z)$ will approach the correlation function $C(k_x, q_y)$ (red line). For q_z (blue lines) the displacements are $d_x = 1, 0$ fm, and for q_x (green lines) the velocity is chosen such that $\gamma v_z/T_s = 1.0$ fm. The values of k_x are for the blue lines: 0.25, 0.5, 0.75, 1.0, 1.25 and 2.0 $[fm]^{-1}$ and for the green lines: 0.25, 0.5, 0.75, 1.0 and 1.5 $[fm]^{-1}$.

The correlation function for different source locations and velocities are similar. The cosine term appears in the same direction as the axis at which the sources are located and the hyperbolic cosine in the direction of the velocity. See Figure 2.5. The zero points discussed for the two static sources at Eq. (2.17), appear in the distributions $C(k_x, q_x)$ and $C(k_y, q_x)$. These distributions do depend on the magnitude of the flow velocity, v_z, but not on its direction! This arises from the fact that the detectors are **assumed to be** reached from both sides of the system with opposite velocities with equal probability.

Unfortunately the dominant direction of flow (see Fig. 2.7) is the beam

direction ($z-$direction), where we have no possibility to place high acceptance detectors. At the same time the strongest effect of the flow appears in this direction.

The rotation in the reaction plane can also be characterized with **another configuration** of the two moving sources, when the displacement is in the z-direction while the flow velocities are pointing into the x-direction, so that the source at $x_1 = d_z$ has a negative velocity, $-v_x$ while the source at $x_2 = -d_z$ has a positive velocity, v_x. The detailed description of the correlation functions from this configuration can be obtained in a straightforward way similarly to the previous case, see Eq. (2.27). In this case the flow has the most dominant effect in the k_x-direction, which is accessible for detection. The x-directed flow, however, is more sensitively dependent on secondary effects, like the Kelvin-Helmholtz Instability [2].

In this configuration of the sources the magnitude of the flow velocity makes visible change in $C(k,q)$, in the (k_x, q_x)-direction also, which is detectable by the usual detector configurations. Still the direction of the rotation does not appear in the observables with the approach presented here.

This actually arises from the simplifying assumption, that the freeze out is happening instantly at a timelike hypersurface with $\sigma^\mu = (1,0,0,0)$, where particles from all sides of the system can reach each detector with the same probability. We will return to this problem after having discussed the more complex source configurations.

$$
\begin{aligned}
C(k_x, q_x) &= 1 + \exp(-R^2 q_x^2)\, \frac{\cosh\left(\frac{2\gamma k_x v_x}{T_s}\right) + \cosh\left(\frac{\gamma q_x v_x}{T_s}\right)}{\cosh\left(\frac{2\gamma k_x v_x}{T_s}\right) + 1}\ , \\
C(k_x, q_y) &= 1 + \exp(-R^2 q_y^2)\ , \\
C(k_x, q_z) &= 1 + \exp(-R^2 q_z^2)\, \frac{\cosh\left(\frac{2\gamma k_x v_x}{T_s}\right) + \cos\left(2 q_z d_z\right)}{\cosh\left(\frac{2\gamma k_x v_x}{T_s}\right) + 1}\ .
\end{aligned}
\tag{2.27}
$$

For these two-particle correlation measurements it is necessary to identify independently, event by event the global collective reaction plane azimuth, Ψ_{RP}, experimentally and the corresponding event by event center of mass of the system (e.g. with the method [27]). Knowing these we can identify the k_x-direction and the k_y-direction also.

In this section we derived a relatively simple formula for two sources with opposite positions and opposite velocities. These kind of systems were analysed earlier for radially expanding systems.

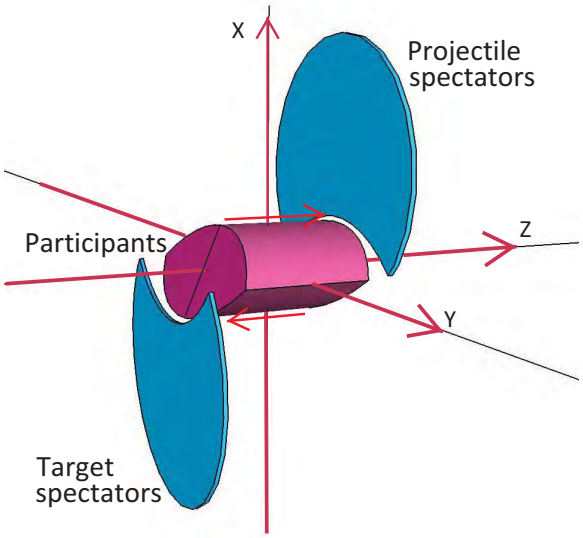

Figure 2.7: (Color online) Typical orientation of the spatial axes in case of an ultra-relativistic heavy ion reaction shortly after the impact. In the configuration space the projectile and target appear to be flat due to the Lorentz contraction.

Recently due to the angular momentum in peripheral heavy ion collisions strong rotation [1] and turbulence (Kelvin-Helmholtz Instability) [2] were predicted in fluid dynamical models arising from the symmetries, shear and vorticity of the initial state.

In the simple two source example shown in the previous section the two sources may describe a rotation if the sources are at a distance from the center in the x-direction, $\mathbf{x}_1 = (+d, 0, 0)$ and $\mathbf{x}_2 = (-d, 0, 0)$, while these have opposite velocities pointing into the z-direction, $\mathbf{u}_1 = \gamma(1, 0, 0, v_z)$ and $\mathbf{u}_2 = \gamma(1, 0, 0, -v_z)$.

It is important to mention that to detect rotation the accurate identification of the reaction plane and its proper orientation is necessary. In the so called "cumulative" methods the reaction plane is identified but its projectile and target sides are not. This makes it impossible to detect directed flow, and odd components of the global collective flow. (All harmonic components

of random fluctuations of course can be detected.) Furthermore, not only the reaction plane with proper direction but also the event by event center of mass (c.m.) should also be identified [27]. This hardly ever done! In both cases the use of zero degree calorimeters are provide an adequate tool as these are sensitive to the spectator residues.

The correlation function depends both on vectors **k** and **q**. To detect rotation the choices should be correlated correctly with the beam and the directed reaction plane as illustrated in Figure 2.7. The positive x-axis points in the direction of the projectile, which moves in the positive direction along the z-axis.

In eq. (2.23), in the above situation, $\mathbf{ku}_s = \gamma k_z v_z$, $\mathbf{qu}_s = \gamma q_z v_z$ and $\mathbf{qx}_s = q_x d$. Thus, the Correlation function, apart of the single cell source size, R, sensitivity, has a specific dependence on k_z and q_z, as well as on q_x. Unfortunately it is difficult to measure the particle momenta in the z-direction as it coincides with the beam. The q_x dependence would enable us to estimate the distance of the two sources.

2.3 Four Fluid Cell Sources

2.3.1 Symmetric source configurations

Four sources as combination of two moving double source systems. We use the same parameters as under paragraph e, where s_1 and s_2 will be the two different pairs of sources with different locations and velocities. See Figure 2.8.

So we have

$$
\begin{aligned}
C(k,q) = exp(-R^2q^2)\times \\
&\left[\cosh\left(\frac{2\mathbf{k}\cdot\mathbf{u}_{s_1}}{T_s}\right) + \cosh\left(\frac{\mathbf{q}\cdot\mathbf{u}_{s_1}}{T_s}\right)\cos(2\mathbf{q}\cdot\mathbf{x}_{s_1}) + \right. \\
&\cosh\left(\frac{2\mathbf{k}\cdot\mathbf{u}_{s_2}}{T_s}\right)\cosh\left(\frac{\mathbf{q}\cdot\mathbf{u}_{s_2}}{T_s}\right)\cos(2\mathbf{q}\cdot\mathbf{x}_{s_2})) + \\
&2\cosh\left(\frac{\mathbf{k}\cdot(\mathbf{u}_{s_1}-\mathbf{u}_{s_2})}{T_s}\right)\cosh\left(\frac{\mathbf{q}\cdot(\mathbf{u}_{s_1}+\mathbf{u}_{s_2})}{2T_s}\right)\cos(\mathbf{q}\cdot(\mathbf{x}_{s_1}+\mathbf{x}_{s_2})) + \\
&\left. 2\cosh\left(\frac{\mathbf{k}\cdot(\mathbf{u}_{s_1}+\mathbf{u}_{s_2})}{T_s}\right)\cosh\left(\frac{\mathbf{q}\cdot(\mathbf{u}_{s_1}-\mathbf{u}_{s_2})}{2T_s}\right)\cos(\mathbf{q}\cdot(\mathbf{x}_{s_1}-\mathbf{x}_{s_2}))\right]\times \\
&\left[\cosh\left(\frac{2\mathbf{k}\cdot\mathbf{u}_{s_1}}{T_s}\right) + \cosh\left(\frac{2\mathbf{k}\cdot\mathbf{u}_{s_2}}{T_s}\right) + 2\cosh\left(\frac{\mathbf{k}\cdot(\mathbf{u}_{s_1}+\mathbf{u}_{s_2})}{T_s}\right) + \right. \\
&\left. 2\cosh\left(\frac{\mathbf{k}\cdot(\mathbf{u}_{s_1}-\mathbf{u}_{s_2})}{T_s}\right) + 2\right]^{-1}
\end{aligned}
\tag{2.28}
$$

If $s_1 = s_2$ then we recover eq. (2.23)

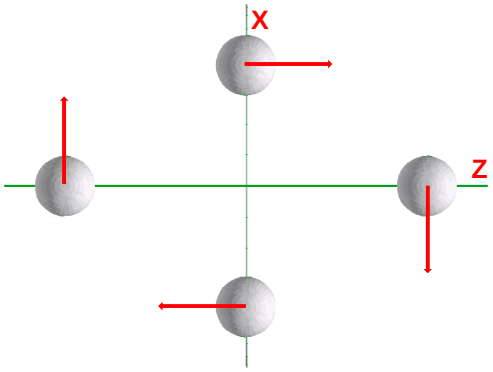

Figure 2.8: (color online) Four moving sources in the reaction ($[x-z]$) plane, one pair, $s1$, is separated in the $x-$ directions and the other, $s2$, is in the $z-$ direction. The sources are moving in the directions indicated by the (red) arrows, $\pm\mathbf{u}_{s1}$ for the 1st pair and $\pm\mathbf{u}_{s2}$ for the other.

In the case of a rotating but symmetric system the displacements and velocities are of equal magnitude and are orthogonal to each other in the two

pairs: $\mathbf{x}_{s_1} \perp \mathbf{x}_{s_2}$ and $\mathbf{u}_{s_1} \perp \mathbf{u}_{s_2}$. Thus a simple sign change of the velocity for one of the pairs or both does not change the result, and so the rotation can be identified, but this evaluation does not provide sensitivity to the direction of the rotation. The reason is in the simplified freeze out assumption as we mentioned already at the end of paragraph 2.2.2.

If the two pairs are not completely identical, i.e. the magnitude of the characteristic quantities of the two source pairs are not equal then a sensitivity to the direction of the rotation may in principle occur. However, if we change the direction of the velocities of the two source pairs simultaneously (as it happens in changing the direction of rotation) the result still does not change.

2.3.2 Four Sources with Flow Circulation

Recent fluid dynamical studies indicate [1, 2], that due to the initial shear and angular momentum the early fluid dynamical development has significant flow vorticity and circulation on the reaction plane. These were recently evaluated [4]. At the present LHC Pb+Pb collision energy in the mentioned fluid dynamical model calculation the maximum value of vorticity, ω, was found exceeding 3 c/fm , and the circulation after 6 fm/c flow development and expansion was still around 4-5 fm·c. This vorticity in the reaction plane was more than an order of magnitude bigger than in the transverse plane estimated from random fluctuations in the transverse plane in ref. [38].

In this section we will look at the four source correlation function with similar circulation as in the above mentioned fluid dynamical model estimates in the reaction plane. See Figure 2.8. We will simulate a circulation value $\Gamma = 5fm \cdot c$. We use eq. (2.28) where the center-of-mass momentum, $\mathbf{k}$ points in the $x - direction$.

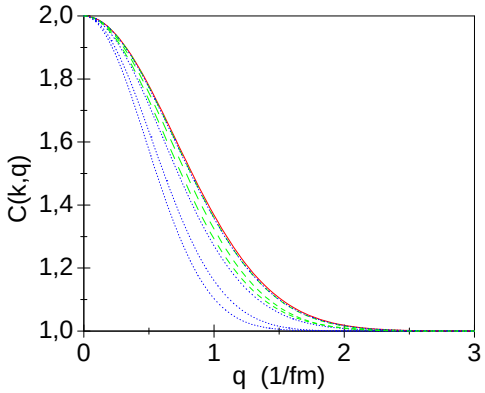

Figure 2.9: (color online) The correlation functions, $C(k,q)$, for 4 sources where the displacement is such that there is one source pair on the x-axis and one the z-axis, the center-of-mass momentum of the emitted particles, $\mathbf{k}$, is in the x-direction. The dotted blue lines are for the velocity $v = 0.5$c and displacement $d_x = d_z = 1.6$fm. The dashed green lines are for the velocity $v = 0.8$c and displacement $d_x = d_z = 1.0$fm. $T_s = 0.20$GeV. In both cases the circulation is $\Gamma = 5fm \cdot c$. The values of k_x are for the blue lines: 0.5, 1.5, 3.0 and 6.0 $[fm]^{-1}$ and for the green lines: 0.5, 1.5 and 3.0 $[fm]^{-1}$. The solid red line is the correlation function $C(k_x, q_y)$. For large values of the center-of-mass momentum k_x the correlation functions $C(k_x, q_x)$ and $C(k_x, q_z)$ will approach the correlation function $C(k_x, q_y)$. The larger displacement and smaller rotation velocity leads to stronger deviation from the unaffected correlation function $C(k_x, q_y)$.

Since the position and velocity are of the same value and because of symmetry the correlation functions $C(k_x, q_x)$ and $C(k_x, q_z)$ provide the same values. So we take the correlation function $C(k_x, q_x)$ and we have after some simplification

$$C(k_x, q_x) = 1 + \exp(-R^2 q^2) \left[1 + \cos(2q_x d) + \cosh\left(2\frac{k_x \gamma v_x}{T_s}\right) + \cosh\left(\frac{q_x \gamma v_x}{T_s}\right) + 4\cosh\left(\frac{k_x \gamma v_x}{T_s}\right)\cosh\left(\frac{q_x \gamma v_x}{2T_s}\right)\cos(q_x d)\right]\left[\cosh\left(\frac{2k_x \gamma v_x}{T_s}\right) + 4\cosh\left(\frac{k_x \gamma v_x}{T_s}\right) + 3\right]^{-1} \tag{2.29}$$

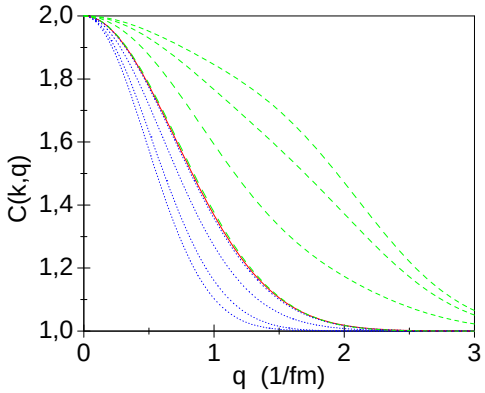

Figure 2.10: (color online) The correlation functions, $C(k,q)$, for 4 sources where the displacement is such that there is one source pair on the x-axis and one the z-axis, the center-of-mass momentum of the emitted particles, $\mathbf{k}$, is in the x-direction. The dotted blue lines are for the velocity $v = 0.5$c and displacement $d_x = d_z = 1.6$fm (same as in the previous figure). The dashed green lines are for the velocity $v = 0.95$c and displacement $d_x = d_z = 0.84$fm. $T_s = 0.20$GeV. The values of k_x are for the blue lines: 0.5, 1.5, 3.0 and 6.0 $[fm]^{-1}$ and for the green lines: 0.1, 0.25, 0.5 and 1.5 $[fm]^{-1}$. The solid red line is the correlation function $C(k_x, q_y)$. For large values of the center-of-mass momentum k_x the correlation functions $C(k_x, q_x)$ and $C(k_x, q_z)$ will approach the correlation function $C(k_x, q_y)$. Now for the dashed green lines with even higher velocity and smaller displacement, the deviation is significantly in the positive direction.

For $C(k_x, q_y)$ we have the same result as we had for the two moving sources. Here the flow and displacement have no effect.

Let us look at comparisons for similar circulations and for similar displacements.

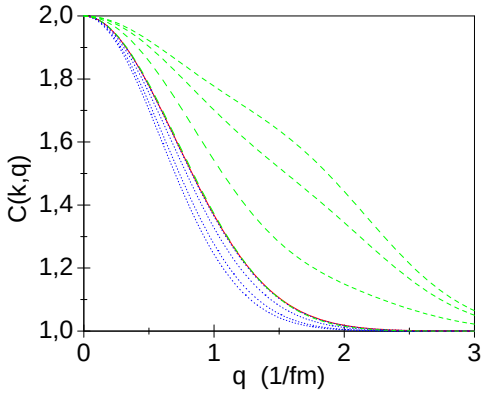

Figure 2.11: (color online) Same figure as the previous one, however the circulation is not the same and the displacements are equal. The dotted blue lines are for the velocity $v = 0.5$c and displacement $d_x = d_z = 1.0$fm. The dashed green lines are for the velocity $v = 0.95$c and displacement $d_x = d_z = 1.0$fm. $T_s = 0.20$GeV. The values of k_x are for the blue lines: 0.5, 1.5, 3.0 and 6.0 $[fm]^{-1}$ and for the green lines: 0.1, 0.25, 0.5 and 1.5 $[fm]^{-1}$. Here the displacement is the same but the ultra-relativistic velocities lead still to the deviation in the positive direction.

By comparing Figures 2.10 and 2.11 we see that an increase in the displacement of the sources gives a increase in the apparent size of the system (narrower $q-$distribution. We also see that the measured size of the system increases with decreasing velocity.

The correlation function is symmetric in all these cases as sources from opposite sides of the system contribute equally. Thus the correlation function is not sensitive to the direction of rotation.

Chapter 3

Asymmetric Sources

We have seen in the previous few source model examples that a highly symmetric source may result in highly symmetric correlation functions, however, this results were not sensitive to the direction of the rotation, which seems to be unrealistic. We saw that this result is a consequence of the assumption that both of the members of a symmetric pair contribute equally to the correlation function even if one is at the side of the system facing the detector and the other is on the opposite side. The dense and hot nuclear matter or the Quark-gluon Plasma are strongly interacting, and for the most of the observed particle types the detection of a particle from the side of the system, – which is not facing the detector but points to the opposite direction, – is significantly less probable. The reason is partly in the diverging velocities during the expansion and partly to the lower emission probability from earlier (deeper) layers of the source from the external edge of the timelike (or spacelike) FO layer. This feature is recognized for a long time and discussed in detail by now. This influences the particle emission (or freeze out (FO)) process and modifies the post FO particle distribution. This topic has an extended literature, and this feature destructs the symmetry of emission of from source pairs at the opposite sides of the system [10, 18, 19, 20, 15, 28, 29, 30, 31, 32, 33, 34, 35, 36, 37].

For the study of realistic systems where the emission is dominated by the side of the system, which is facing the detector, we cannot use the assumption of the symmetry among pairs or groups of the sources from opposite sides of the system. Even if the FO layer has a time-like normal direction, $\hat{\sigma}^\mu$ the $(k^\mu \hat{\sigma}^\mu)$ factor yields a substantial emission difference between the opposite sides of the system. Now we want to demonstrate this effect on few source

examples, and we will demonstrate the consequences of the non-symmetric emission.

3.1 The Emission Probability

It was first recognized that the freeze out with the Cooper-Fry description [15], may lead to negative contributions for particles, which move towards the center of the system and not in the direction out, towards the detectors. The first proposal to remedy this problem came from Bugaev [29], which led to the introduction of an improved post freeze out distribution in the Cooper-Frye description, first with the Cut-Jüttner distribution [29, 31] and then by the Cancelling-Jüttner distribution [35].

Subsequently it was realized that for the realistic treatment of the freeze out process in transport theory one has to modify the Boltzmann transport equation by replacing the local molecular chaos assumption with a non-local one, where the point of origin is also included in the phase space distributions of the colliding particles. This led to the Modified Boltzmann Transport equation (MBT), and also the necessity to introduce an escape probability, P_{esc} was pointed out.

The escape probability was then introduced and analysed in a series of publications [18, 19, 20, 37], in transport theoretical approaches. It was pointed out that even if the pre FO distribution is a locally equilibrated isotropic distribution, the freeze out process and the escape probability will provide a nonisotropic distribution which eliminates the earlier observed problems. This developing anisotropy in the freeze out process occurs for freeze out both in space-like and time-like directions.

The escape probability introduced in the works [18, 19, 20, 37], for a space-time surface layer of the system of thickness L, pointing in the four direction $\hat{\sigma}^\mu$ was given at a point x^μ inside the freeze out layer as

$$P_{esc}(x) \;\propto\; \left(\frac{L}{L - x^\mu \hat{\sigma}_\mu}\right) \left(\frac{p^\mu \hat{\sigma}_\mu}{p^\mu u_\mu}\right) \Theta(p^\mu \hat{\sigma}_\mu)\,, \tag{3.1}$$

where p^μ is the momentum of the escaping particle, $u^\mu(x)$ is the local flow velocity and $s = x^\mu \hat{\sigma}_\mu$ is the distance of the emission point from the inside boundary of the layer. The first multiplicative term describes higher emission probability to the particles, which are emitted closer to the outside boundary of the layer, the second multiplicative term describes the higher

emission probability for the particles, which move in the normal direction of the surface, because these should cross less material in the layer. The last term secures that only those particles can escape, which move outwards through the layer.

The last two momentum dependent factors are important in transport theoretical models, to determine the shape of the post FO momentum distribution, e.g. [35], which would replace the Jüttner distribution. This shape modification happens to the single and two particle distributions equally, and it acts in all emission directions, $\mathbf{k}$, equally, so this effect is secondary from the point of view of the flow velocity dependence of the correlation function.

In order to describe the complete freeze out process for a reaction the system had to be surrounded with a freeze out layer in the space-time, and the phase space distribution of the escaping, frozen out particles can be obtained by integrating over the whole 4-volume of the freeze out layer the local (usually isotropic) phase space distribution with the escape probability $P_{esc}(x)$. This procedure would then play the role of function $G(x)$ in the source function in eq. (1.10) instead of the simplified assumptions, as e.g. in eq. (1.14).

The correlation function, $C(k,q)$ is always measured in a given direction of the detector, $\mathbf{k}$. Obviously only those particles can reach the detector, which satisfy $k^\mu \hat{\sigma}_\mu > 0$. Thus in the calculation of $C(k,q)$ for a given $\hat{\mathbf{k}}$- direction we can exclude the parts of the freeze out layer where $k^\mu \hat{\sigma}_\mu < 0$ (see eq. (10) of ref. [10] or ref. [29]). For time-like FO a simplest approximation for the emission possibility is $P_{esc}(x) \propto k^\mu u_\mu(x)$ [21].

In a model calculation we therefore have to define the freeze out layer also, this realistically should not include the whole space-time volume of the reaction. In case of calculating $C(k,q)$ for a given $\hat{\mathbf{k}}$ we should select the relevant part of the freeze out layer, which may contribute to emission in the $\mathbf{k}$ direction. This should be a layer of 2-3 m.f.p facing the detector at the direction $\hat{\mathbf{k}}$. This can eliminate the symmetric pairs of fluid cells in the previous calculations of the correlation function, even if the emission normal is timelike, because the FO particle from an earlier emission point in the ST has to propagate through the plasma for some finite time, with considerable quenching.

Therefore in the following models we should apply the escape probability and we should define a $\hat{\mathbf{k}}$-dependent freeze out layer also! The most simple approximation is to select an emission layer from the system for a given $\hat{\mathbf{k}}$-direction with uniform emission probability from within this layer. The

next to most simple approximation is to introduce an emission probability within the layer, increasing towards the outside boundary of the layer. (Here it is important to mention that the spatial emission probability should be sufficiently smooth, so that one fluid cell and its contribution to $C(k,q)$, should not be effected by this emission probability.

When we have up to 4 sources we can always add $\hat{\mathbf{k}}$-dependent emission weights to these sources. This still would qualitatively change the outcome. As we discuss here up to four sources only a detailed formal evaluation of the emission probability would be an exaggerated approach, by defining more parameters than the outcome, so we just define the weights themselves here. In a full 3+1D fluid dynamical model with 100000+ fluid cells of course we have to apply a realistic and general evaluation of emission probability for every point of the ST.

3.2 Emission probabilities for few sources

3.2.1 Two sources

The previous discussion included two sources (i) in the beam-, $z-$direction and (ii) in the transverse direction in the reaction plane, $x-$direction. In case (i) the emission could be different from the two sources if the detector is in the $z-$ direction, which is difficult to achieve, so we do not have to discuss this possibility.

In configuration (ii) the observation can be in different $\hat{\mathbf{k}}$-directions. If $\hat{\mathbf{k}}$ points into the $\pm y-$direction, then the probabilities must be identical so emission probabilities do not lead to any change.

If $\hat{\mathbf{k}}$ points into the $\pm x-$direction, then one of the sources is closer to the detector and may shadow the more distant one. Thus, we can just introduce two positive weight factors so that w_c is the weight for the cells closer to the detector and w_s is for the cells which are far from the detector measuring the average momentum $\mathbf{k}$. These weights are the same for the calculation of the nominator and denominator of the correlation function, so their normalization does not influence the correlation function.

As not all emitted particles reach a given detector the normalization is also dependent on the direction of the detector. Thus, we evaluate the correlation function this way. This immediately changes the earlier result (2.24), because it breaks the symmetry between the two sources. We can simply repeat the

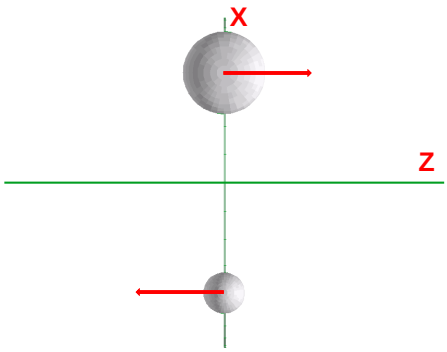

Figure 3.1: (color online) Two moving sources in the reaction ($[x-z]$) plane, separated in the $x-$ direction (case (ii) in the text. The sources are moving in the directions indicated by the (red) arrows. The detector is in the positive $x-$direction, thus the source on this side has more dominant emission into this direction, and this is indicated by the bigger size of the source on this side.

calculation for two moving sources in section 2.2.2, modifying the derivation of eq. (2.22) and obtain the general result

$$C(k,q)\Big|_{+x} = 1+\exp(-R^2q^2)\,\frac{w_c^2 e^{\frac{2\mathbf{k}\mathbf{u}_s}{T_s}} + w_s^2 e^{-\frac{2\mathbf{k}\mathbf{u}_s}{T_s}} + 2w_c w_s \cosh\left(\frac{\mathbf{q}\mathbf{u}_s}{T_s}\right)\cos(2\mathbf{q}\mathbf{x}_s)}{w_c^2 e^{\frac{2\mathbf{k}\mathbf{u}_s}{T_s}} + w_s^2 e^{-\frac{2\mathbf{k}\mathbf{u}_s}{T_s}} + 2w_c w_s}\,. \tag{3.2}$$

Note that this result is valid for the case when $\hat{\mathbf{k}}$ points to the $+x$ direction, because the weights depend on this and $w_c > w_s$. See Figure 3.1. The fact that the emission from the source, which is closer to the detector is stronger makes the direction of the flow detectable.

If we introduce the notation $w_c = 1+\epsilon$ and $w_s = 1-\epsilon$, the deviation from the symmetric result will become apparent

$$C(k,q)\Big|_{+x} = 1+\exp(-R^2q^2)\times \frac{(1+\epsilon^2)\cosh\left(\frac{2\mathbf{k}\mathbf{u}_s}{T_s}\right) + 2\epsilon\sinh\left(\frac{2\mathbf{k}\mathbf{u}_s}{T_s}\right) + (1-\epsilon^2)\cosh\left(\frac{\mathbf{q}\mathbf{u}_s}{T_s}\right)\cos(2\mathbf{q}\mathbf{x}_s)}{(1+\epsilon^2)\cosh\left(\frac{2\mathbf{k}\mathbf{u}_s}{T_s}\right) + 2\epsilon\sinh\left(\frac{2\mathbf{k}\mathbf{u}_s}{T_s}\right) + (1-\epsilon^2)}\,. \tag{3.3}$$

If $\epsilon \to 0$, i.e. if $w_c = w_s$, we recover the earlier result, eq. (2.23).

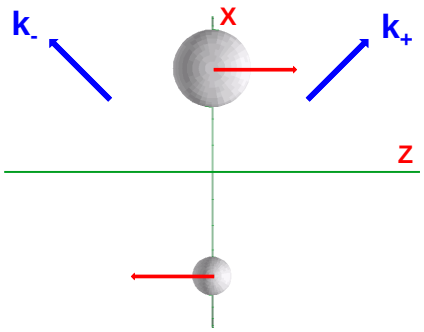

Figure 3.2: (color online) Two moving sources in the reaction ($[x-z]$) plane, separated in the $x-$ direction. The sources are moving in the directions indicated by the (red) arrows. The two "tilted" detector directions are indicated by the (blue) arrows labeled with k_+ and k_-.

If $\epsilon = 0$ we have the symmetric situation where both sources have equal contribution, the asymmetric terms vanish, and the result becomes to be symmetric for the change of the direction of the flow velocity. If ϵ reaches its maximal value, $\epsilon = 1$ the contribution of the far side source is eliminated ($w_s = 0$, $w_c = 2$), and only the single nearby source contributes to the correlation function. In this case the asymmetric term in the nominator vanishes, the remaining terms in the nominator and denominator are equal, and we recover the single static source result.

This result has terms, which change sign if the flow velocity, $\mathbf{u}_s$ changes sign. The result is valid only if the detector is in the $\hat{\mathbf{k}} = (1, 0, 0)$ direction. For this direction, however, if the flow velocity points in the z-direction, i.e. orthogonal to $\mathbf{k}$ the asymmetric term does not provide any contribution, so it will not show up in $C(k_x, \mathbf{q})$. To circumvent this problem we should study detector directions, which do not coincide with the primary axes of the given event (where x is the direction of the impact parameter vector, $\mathbf{b}$, pointing to the projectile; y is the other transverse direction; and z is the direction of the projectile beam).

3.2.2 Correlation in Tilted Directions

The form of the correlation function is the same if $\mathbf{k}$ is in the same plane, the reaction plane, but it has a z component also, i.e. $\mathbf{k} = (k_x, 0, \pm k_z)$.

This is possible for all LHC heavy ion experiments, ATLAS, CMS and even ALICE, where the longitudinal acceptance range of the TPC ($\Delta\eta < 0.8$) is the smallest.

Earlier for spherically or longitudinally expanding systems the dependence of the correlation function on the tilt angle or *width* parameter was analysed in detail in ref. [10]. We do not go into similar fine details, just demonstrate the possibilities for an arbitrary configuration.

Depending on the detector acceptance we should chose a detector direction where $|k_z|$ is as big as the detector acceptance allows it. For this configuration the **form** of the correlation function is the same as (3.3)

$$C(k,q)\Big|_{+x,\pm z} = C(k,q)\Big|_{+x}, \tag{3.4}$$

with keeping the different weights, w_c, w_s or ϵ so that the forward shifted and backward shifted directions have the same weights. These weights are not specified up to now anyway.

For detection of the correlation function we have to introduce here the usual, **k**-dependent coordinate system to classify the direction of **q**. Thus if

$$\hat{\mathbf{k}}_{\pm} = (a, 0, \pm b)\mathrm{fm}^{-1},\ k_x = a|\mathbf{k}|,\ k_z = \pm b|\mathbf{k}|, \tag{3.5}$$

where $a^2 + b^2 = 1$. Then the difference vector, **q**, can be measured in the directions

$$\begin{aligned}
&\hat{\mathbf{q}}_{out} = (a, 0, \pm b),\ q_x = a|\mathbf{q}|,\ q_z = \pm b|\mathbf{q}| \\
&\hat{\mathbf{q}}_{side} = (0, 1, 0), \quad q_y = |\mathbf{q}| \\
&\hat{\mathbf{q}}_{long} = (\mp b, 0, a), \quad q_x = \mp b|\mathbf{q}|,\ q_z = a|\mathbf{q}|.
\end{aligned} \tag{3.6}$$

This leads to the following correlation functions

$$
\begin{aligned}
&C(k_{(\pm)}, q_{out}) = 1 + \exp(-R^2 q^2) \times \\
&\frac{(1{+}\epsilon^2)\cosh\left(\frac{2\gamma k_z v_z}{T_s}\right) + 2\epsilon\sinh\left(\frac{2\gamma k_z v_z}{T_s}\right) + (1{-}\epsilon^2)\cosh\left(\frac{\gamma q_z v_z}{T_s}\right)\cos\left(q_x d_x\right)}{(1{+}\epsilon^2)\cosh\left(\frac{2\gamma k_z v_z}{T_s}\right) + 2\epsilon\sinh\left(\frac{2\gamma k_z v_z}{T_s}\right) + (1{-}\epsilon^2)} \ , \\
&C(k_{(\pm)}, q_{side}) = 1 + \exp(-R^2 q^2) \ , \\
&C(k_{(\pm)}, q_{long}) = 1 + \exp(-R^2 q^2) \times \\
&\frac{(1{+}\epsilon^2)\cosh\left(\frac{2\gamma k_z v_z}{T_s}\right) + 2\epsilon\sinh\left(\frac{2\gamma k_z v_z}{T_s}\right) + (1{-}\epsilon^2)\cosh\left(\frac{\gamma q_z v_z}{T_s}\right)\cos\left(q_x d_x\right)}{(1{+}\epsilon^2)\cosh\left(\frac{2\gamma k_z v_z}{T_s}\right) + 2\epsilon\sinh\left(\frac{2\gamma k_z v_z}{T_s}\right) + (1{-}\epsilon^2)} \ .
\end{aligned}
\tag{3.7}
$$

Although, it seems that $C(k_{(\pm)}, q_{out})$ and $C(k_{(\pm)}, q_{long})$ are the same, this is in fact not the case, because the values of the components of the different types of $\mathbf{k}$ and $\mathbf{q}$ are not the same as described in eqs. (3.5,3.6). In all cases, the out-, side- and long- $q = |\mathbf{q}|$. We will also use the notation $k = |\mathbf{k}|$ and $\gamma v_x = u_x$, $\gamma v_y = u_y$, $\gamma v_z = u_z$, so that $\mathbf{u}_s = (u_x, u_y, u_z)$. For example for the *out* component the difference of the forward and backward shifted correlation functions is

$$
\begin{aligned}
&\Delta(k_\pm, q_{out}) \equiv C(k_+, q_{out}) - C(k_-, q_{out}) = \\
&\frac{4\exp(-R^2 q^2)\ \epsilon\sinh\left(\frac{2u_z\, bk}{T_s}\right)\ (1{-}\epsilon^2)\left[1 - \cosh\left(\frac{u_z\, bq}{T_s}\right)\cos\left(aqd_x\right)\right]}{\left[(1{+}\epsilon^2)\cosh\left(\frac{2u_z\, bk}{T_s}\right) + (1{-}\epsilon^2)\right]^2 - 4\epsilon^2\sinh^2\left(\frac{2u_z\, bk}{T_s}\right)} .
\end{aligned}
\tag{3.8}
$$

As eq. (3.8) and Fig. 3.3 show, the Differential Correlation Function (DCF), $\Delta(k_\pm, q_{out})$, is sensitive to the speed and direction of the rotation, and it is also sensitive to the amount of the tilt in the directions of the detection, regulated by the parameters a and b. $\Delta(k_\pm, q_{out})$ tends to zero both if $q \to 0$ and if $q \to \infty$. The structure of $\Delta(k_\pm, q_{out})$ is determined by the $\cosh\left(u_z b\, q/T_s\right)\cos\left(ad_x\, q\right)$ product. If in both arguments the coefficients of q, $u_z b/T_s$ and ad_x are positive, smaller than one, and $u_z b/T_s \leq ad_x$, then the DCF is positive. If the coefficient ad_x exceeds one the cos function changes sign at high q_{out} values (e.g. above $q = 1 - 2\mathrm{fm}^{-1}$), and the DCF becomes

negative at high q_{out} values. Note that the ratio of the two coefficients is influenced be the choice of the tilting angle, i.e. by the parameters a and b.

If the parameter ad_x remains constant, about 1 fm, and then when $u_z b/T_s$ becomes larger (than one) the Differential Correlation Function becomes negative at small q values.

If the parameter $u_z b/T_s$ remains constant, and about 1 fm, then when ad_x becomes less (than one) the DCF becomes negative at small q values.

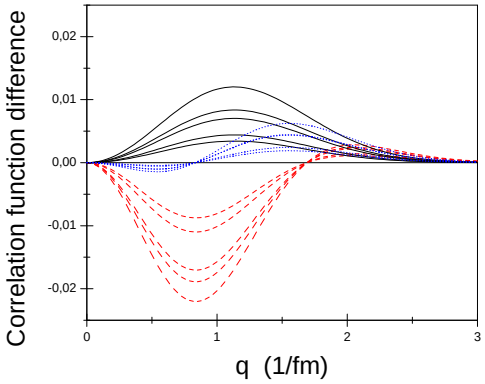

Figure 3.3: (color online) Difference of the forward and backward shifted correlation function, $\Delta(k_{\pm}, q_{out})$, for the value $\epsilon = 0.50$. The solid black lines is for the velocity $v_z = 0.5$c, dotted blue lines are for the velocity $v_z = 0.6$c and dashed red lines are for the velocity $v_z = 0.7$c. Displacement $d_x = 1.0$fm, $T_s = 0.139$GeV and $a = b = \frac{1}{\sqrt{2}}$. The values of k are for the solid black lines: 0.25, 0.50, 2.00, 2.75 and 3.50 $[fm]^{-1}$, the dotted blue lines: 0.25, 0.50, 1.00, 1.75 and 2.50 $[fm]^{-1}$, and the dashed red lines: 0.25, 0.50, 0.75, 1.25 and 1.75 $[fm]^{-1}$.

If we change the direction of rotation to the opposite the Differential Correlation Function changes sign due to the sinh function in the nominator. In this configuration with the change of the tilt of the detector directions we can adjust the DCF, tot he threshold value where the $\Delta(k_{\pm}, q_{out})$, is still positive, which provides a sensitive estimate for the rotation velocity at Freeze Out.

This very sensitive behaviour is rather special and it appears in this special two source model this way. With an increased resolution and with more source elements this strong and specific structure will be smoothed out to

some extent.

The $\sinh(2u_z\, bk/T_s)$ term changes sign in the nominator when u_z changes sign the difference of the two correlation functions, $\Delta(k_\pm, q_{out})$ changes sign also because all other terms are symmetric to the sign change of the velocity.

This is an important observation as we can detect the direction and magnitude of the rotation in the reaction plane. This difference is also increasing with the longitudinal shift, b, of the average momentum vector, $\mathbf{k}$, so that detectors with larger pseudorapidity acceptance can detect the rotation better.

In order to perform this measurement, one has to determine the global reaction plane (e.g. from spectator residues in the ZDCs), and determine the projectile side of this plane. Furthermore the event by event center of mass should also be identified (using e.g. the method shown in ref. [27]). This will be the positive x-direction. Then the correlation function can be measured for four different $\mathbf{k}$-directions in the global reaction plane. These four directions are shifted forward and backward from the center of mass symmetrically on the projectile side, and there should be a symmetric pair of detection points in the target side of the reaction plane too.

The $\mathbf{k}$ directions opposite to each other across the c.m. point give the same result, while the difference, $\Delta(k_\pm, q_{out})$, between the Forward (F) and Backward (B) shifted contributions will characterize the speed and direction of the rotation. This symmetry can be used to eliminate the contribution from eventual random fluctuations. The observed F/B asymmetry depends on the parameters ϵ, v_z and d_x, these can be estimated by measuring the correlation functions at all possible moments $\mathbf{k}$.

Figure 3.3 indicates that the differential correlation function has a larger amplitude for smaller k values, and the zero points are sensitively dependent on the rotation velocity.

The zero points come from the term

$$1 - \cosh\left(\frac{u_z bq}{T_s}\right)\cos(aqd_x) = 0 \tag{3.9}$$

and it is not dependent on k, so for the values used in Fig. 3.3 and $q = x\,\mathrm{fm}^{-1}$ we have

$$\cosh\left(\frac{0.197}{0.139}\frac{v_z/c}{\sqrt{1-v_z^2/c^2}}\frac{x}{\sqrt{2}}\right)\cos\left(\frac{x}{\sqrt{2}}\right) = 1\ . \tag{3.10}$$

Since the cosine term must be positive, there are no zero points for $\pi/\sqrt{2} \leq x \leq 3\pi/\sqrt{2}$ or $2.23 \leq x \leq 6.66$.

For $x > 3\pi/\sqrt{2}$ the $\exp(-R^2x^2)$ term will be small and there would be no correlation difference. So we will look at the values $0 < x < \pi/\sqrt{2}$

If v_z is smaller than $0.57c$ then there will be no zero point for $0 < x < \pi/\sqrt{2}$. For v_z larger than $0.58c$ there will be 1 zero point for $0 < x < \pi/\sqrt{2}$.

The zero point for a given velocity can be found by solving equation (3.10) numerically. For velocities $v = 0.6c$ and $v = 0.7c$ we have zero points at $q = 0.83\, fm^{-1}$ and $q = 1.69\, fm^{-1}$ respectively.

This indicates the sensitivity of the method and the possibility to influence it by the choice of the detector directions (via the choice of a and b).

3.3 Emission from four sources

With four sources we can illustrate the possibilities of differential HBT method studies in different directions. The correlation functions can be calculated in general for four sources and two detector positions. This can then be applied to different detector configurations.

Two examples on different detector configurations are given in Figures (3.4-3.5) and (3.6). We use the same equations as in the two source model, eqs. (3.5) and (3.6).

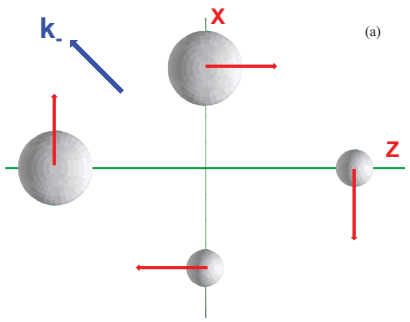

Figure 3.4: (color online) Four moving sources in the reaction ($[x-z]$) plane, separated in the $x-$ and $z-$ directions. The sources are moving in the directions indicated by the (red) arrows. The "tilted" detector direction(s) are indicated by the (blue) arrows.

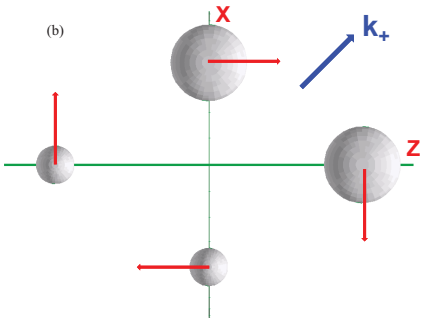

Figure 3.5: (color online) Four moving sources in the reaction ($[x-z]$) plane, separated in the $x-$ and $z-$ directions. The sources are moving in the directions indicated by the (red) arrows. The "tilted" detector direction(s) are indicated by the (blue) arrows.

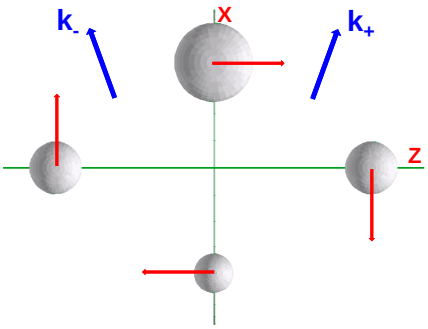

Figure 3.6: (color online) Four moving sources in the reaction ($[x-z]$) plane, separated in the $x-$ and $z-$ directions. The sources are moving in the directions indicated by the (red) arrows. The "tilted" detector direction(s) are indicated by the (blue) arrows.

The details of the calculation are presented in Appendix B.

The out component of the four source correlation function with weight factors ω_a, ω_b, ω_c, ω_d is given by

$$
\begin{aligned}
&C(k_{(\pm)}, q_{out}) = 1 + \exp(-R^2 q^2)\ [2\omega_a\omega_b + 2\omega_c\omega_d + \\
&\omega_a^2 \exp\left(\pm\frac{2\gamma v_z bk}{T_s}\right) \exp\left(\pm\frac{\gamma v_z bq}{T_s}\right) \cos(2ad_x q) + \\
&\omega_b^2 \exp\left(\mp\frac{2\gamma v_z bk}{T_s}\right) \exp\left(\mp\frac{\gamma v_z bq}{T_s}\right) \cos(2ad_x q) + \\
&\omega_c^2 \exp\left(\frac{2\gamma v_x ak}{T_s}\right) \exp\left(\frac{\gamma v_x aq}{T_s}\right) \cos(2bd_z q) + \\
&\omega_d^2 \exp\left(-\frac{2\gamma v_x ak}{T_s}\right) \exp\left(-\frac{\gamma v_x aq}{T_s}\right) \cos(2bd_z q) + \\
&2\omega_a\omega_c \exp\left(\pm\frac{\gamma v_z bk}{T_s}\right) \exp\left(\pm\frac{\gamma v_z bq}{2T_s}\right) \exp\left(\frac{\gamma v_x ak}{T_s}\right) \exp\left(\frac{\gamma v_x aq}{2T_s}\right) \cos((ad_x \pm bd_z)q) + \\
&2\omega_b\omega_d \exp\left(\mp\frac{\gamma v_z bk}{T_s}\right) \exp\left(\mp\frac{\gamma v_z bq}{2T_s}\right) \exp\left(-\frac{\gamma v_x ak}{T_s}\right) \exp\left(-\frac{\gamma v_x aq}{2T_s}\right) \cos((ad_x \pm bd_z)q) + \\
&2\omega_a\omega_d \exp\left(\pm\frac{\gamma v_z bk}{T_s}\right) \exp\left(\pm\frac{\gamma v_z bq}{2T_s}\right) \exp\left(-\frac{\gamma v_x ak}{T_s}\right) \exp\left(-\frac{\gamma v_x aq}{2T_s}\right) \cos((ad_x \mp bd_z)q) + \\
&2\omega_b\omega_c \exp\left(\mp\frac{\gamma v_z bk}{T_s}\right) \exp\left(\mp\frac{\gamma v_z bq}{2T_s}\right) \exp\left(\frac{\gamma v_x ak}{T_s}\right) \exp\left(\frac{\gamma v_x aq}{2T_s}\right) \cos((ad_x \mp bd_z)q)\Bigg] \times \\
&\left[\omega_a \exp\left(\pm\frac{\gamma v_z bk}{T_s}\right) + \omega_b \exp\left(\mp\frac{\gamma v_z bk}{T_s}\right) + \omega_c \exp\left(\frac{\gamma v_x ak}{T_s}\right) + \omega_d \exp\left(-\frac{\gamma v_x ak}{T_s}\right)\right]^{-2} .
\end{aligned}
\tag{3.11}
$$

A source with a larger weight factor is closer to the detector, so that ω_a, ω_b, ω_c, ω_d correspond to $\mathbf{x}_s \equiv (r_x, r_z) = (d_x, 0), (-d_x, 0), (0, d_z), (0, -d_z)$ respectively.

In case if the detector has a narrow pseudorapidity acceptance, then $\mathbf{k}_\pm$ is close to k_x, i.e. $b \ll a$ and then the weights are maximal for the source in the $x-$direction, as indicated in Figure 3.6.

In case if the detector has a wide pseudorapidity acceptance, then $\mathbf{k}_\pm$ can deviate significantly from k_x, i.e. $b \geq a$ and then the weights are maximal for the two sources closest to $\mathbf{k}_+$ or $\mathbf{k}_-$ as indicated in Figures 3.4 and 3.5.

Eq. (3.11) can be used to find the difference of the forward and backward shifted correlation function. We will use that $d_x = d_z$, $v_x = v_z$ and $a = b$.

Some examples for the differential correlation functions are shown in the following Figures 3.7 - 3.8.

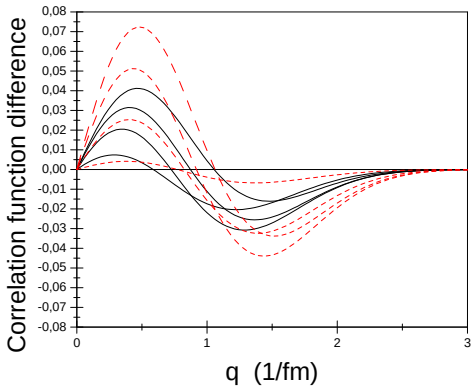

Figure 3.7: (color online) Correlation function difference for the weight factors: $\omega_a = 1.25$, $\omega_b = 0.75$, $\omega_c = \omega_d = 1.00$ for sources placed at $+x$, $-x$, $+z$ and $-z$ respectively. This weight distribution corresponds to the configuration shown in Figure (3.6). The solid black lines are for the velocity $v_z = 0.5$c, and the dashed red lines are for the velocity $v_z = 0.7$c. Displacement $d_x = d_z = 1.0$fm, $T_s = 0.139$GeV and $a = b = \frac{1}{\sqrt{2}}$. The values of k are for the solid black lines: 0.10, 0.50, 1.00, and 2.00 $[fm]^{-1}$ and for the dashed red lines: 0.10, 0.50, 1.00, and 2.00 $[fm]^{-1}$. The difference is larger for smaller values of k.

We can compare Fig. 3.7 with the previously shown two source model, Fig. 3.3, and we see that the amplitudes are similar but the shapes are different. First of all the sensitivity on the direction of rotation remained the same as in the simpler two source model. The two extra sources, c and d lead to higher amplitude for the Differential Correlation Function, while the regular positions of the locations of the zero points are varying due to more sources with different weight parameters.

This configuration can be applied in detectors where the pseudorapidity acceptance range of the detector is not wide. Still the rotation is well detectable. In this configuration the accurate determination of the reaction plane and the participant center of mass momentum is more important.

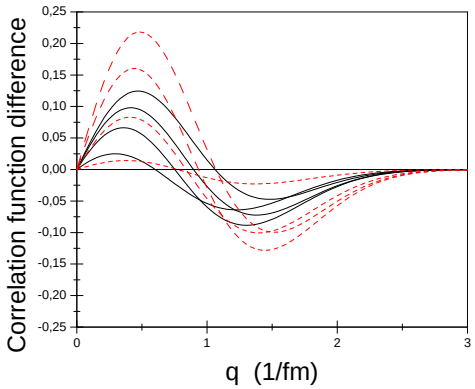

Figure 3.8: (color online) Correlation function difference for the weight factors: $\omega_a = 1.25$, $\omega_b = 0.75$, $\omega_c = 1.50$, $\omega_d = 0.50$ for sources placed at $+x$, $-x$, $+z$ and $-z$ respectively (Fig. 3.5). And $\omega_a = 1.25$, $\omega_b = 0.75$, $\omega_c = 0.50$, $\omega_d = 1.50$ for sources placed at $+x$, $-x$, $+z$ and $-z$ respectively (Fig. 3.4). The solid black lines is for the velocity $v_z = 0.5$c, and the dashed red lines are for the velocity $v_z = 0.7$c. Displacement $d_x = d_z = 1.0$fm, $T_s = 0.139$GeV and $a = b = \frac{1}{\sqrt{2}}$. The values of k are for the solid black lines: 0.10, 0.50, 1.00, and 2.00 $[fm]^{-1}$ and for the dashed red lines: 0.10, 0.50, 1.00, and 2.00 $[fm]^{-1}$. The difference is larger for smaller values of k.

If the detector acceptance is wider, then the two detectors can be placed at more different angles. This configuration makes the forward and backward placed sources more accessible to the forward and backward detectors, respectively. This is taken into account in the emission weights of our sources. These weights are now different for the two components of the DCF!

The result shows the tendency that the DCF has a similar structure as the two source model and the four source model in a resembling configuration. Fig. 3.8 has the same shape as Fig. 3.7, but the amplitude is larger.

For a set of large number of sources, forming a system with close to perfect rotational symmetry, a single correlation function would not depend on the (polar) angle of the detection, and the DCF would vanish. Thus, the DHBT method would not be applicable for highly symmetric systems, like for a rotating star observed from within the plane of the rotation.

At the same time for a rotating binary star system the DHBT method would work. Also the weighting of the sources should be different: If the observer is in the plane of rotation, the distant star is shadowed by the

front one at some periods, just like emission from a highly opaque plasma (evidenced by jet quenching). If the observer is slightly out of the plane of rotation then the two stars are visible all the time and then the (time dependent) correlation function would change between the configurations of Figs. 4 and 7. This also illustrates the role of symmetric and asymmetric weightings.

The rotating and expanding final state of a relativistic heavy ion reaction is of course does not look like a perfect wheel, so the four source model is a more adequate approximation than a wheel would be.

Chapter 4

Computational Fluid Dynamics

We have seen earlier that different one, two and four source systems were tested with and without rotation, as well as, it was discussed in detail what are the consequences if all sources may reach detector equally probable, or if due to the opacity of the source, the fluid elements which are closer and facing the detector have a larger probability to emit a particle towards the detector.

Here we study only the second, realistic case where the emission is *asymmetric* and dominated by the fluid elements facing the detector.

4.1 Flow Symmetries

In numerical fluid dynamical studies of symmetric (A+A) nuclear collision the initial state is symmetric around the center of mass (c.m.) of the system, and (if we do not consider random fluctuations) this symmetry is preserved during the fluid dynamical evolution.

Let us consider the usual conventions, z is the beam axis, and the positive z-direction is the direction of the projectile beam. The impact parameter vector points into the positive x-direction, i.e. towards the projectile. Finally the y-axis is orthogonal to both, so that the x, y, z system is right-handed.

Thus, the situation is similar to the previously discussed case, where on the opposite side of the reaction plane there is a pair to each fluid cell at the point $(t, -x, -y, -z)$. We can conclude that the fluid dynamical system, without fluctuations can be considered as a set of symmetric pairs of fluid cells, assuming that our detector receives particles from each of the sources of

a symmetric pair with equal probability. With this assumption our result will only contain even functions of the flow velocities as in the earlier discussed 2-source and 4-source systems.

In the realistic asymmetric case the emission probability from the two fluid cells of a source pair are are not equal, so the exponentials cannot be reduced to cosh-functions because of the different weights.

If we have several sources, s, with Gaussian space and time profiles, then the source function in Jüttner approximation is

$$\int d^4x\, S(x,k) = \sum_s \int d^3x_s\, dt_s\, S(x_s,k) = \\ (2\pi R^2)^{3/2} \sum_s \frac{\gamma_s n_s(x)\,(k_\mu\,\hat{\sigma}_s^\mu)}{C_s}\, \exp\left[-\frac{k\cdot u_s}{T_s}\right]\,, \tag{4.1}$$

where the spatial integral over a cell volume is, $V_{cell} = (2\pi R^2)^{3/2}$ while the time integral is normalized to unity. Similarly the J-function is

$$J(k,q) = \sum_s \exp\left[-\frac{q\cdot u_s}{2T_s}\right] \exp(iqx_s) \int_S d^4x\; S_s(x,k)\, \exp(iqx)\;. \tag{4.2}$$

We then assume that the FO layer is relatively narrow compared to spatial spread of the fluid cells, so that the peak emission time, t_s, of all fluid cells are the same. Then the $\exp(iq^0 t_s)$ factor drops out from the $J(k,q)J(k,-q)$ product. (If the emission is happening through a layer with timelike normal, but the peak is not at constant t_s, but rather at constant τ_s, then we can adapt the coordinate system accordingly, i.e. we can use the τ,η coordinates instead of t,z, see e.g. [21]). This simplification is justified in case of rapid and simultaneous hadronization and freeze out from the plasma, else for dilute and transparent matter the correlations from the time dependence of freeze out should be handled the same way as the spatial dependence.

Due to the symmetries of the pre-collision initial state the system is mirror symmetric with respect to the $[x,z]$, reaction plane. Thus, it is sufficient to describe the cells on the positive side of the y-axis, because the other side is the mirror image of the positive side. Then we can evaluate the correlation function the same way as we have done earlier.

Thus we define the quantities:

$$\begin{aligned} Q_c &= \left(2\pi R^2\right)^{3/2} \exp\left[-\frac{R^2 q^2}{2}\right], \\ P_s &= \frac{\gamma_s n_s}{C_s} \exp\left[-\frac{k^0\, u_s^0}{T_s}\right], \\ Q_s &= P_s \exp\left[-\frac{q^0\, u_s^0}{2T_s}\right], \\ w_s &= (k_\mu\, \hat{\sigma}_s^\mu)\ \exp\left[-\frac{\Theta_s^2}{2}(q_\mu\, \hat{\sigma}_s^\mu)^2\right]\ , \end{aligned} \tag{4.3}$$

where $u_s^0 = \gamma_s$, the local 4-direction normal of the mean particle emission from an ST point of the flow is $\hat{\sigma}_s^\mu$ (assumed to be time-like), R is the size (radius) of the fluid cells, and Θ_s is the path length of the time integral from the ST point of the source, s, while assuming a Gaussian emission time profile.

We can reassign the summation for pairs, so that $s = \{i, j, k\}$ will correspond to a pair of cells: at $\{i, j, k\}$ and its reflected pair across the c.m. point at the same time at $\{i^*, j^*, k^*\}$. Then the function $S(k, q)$ becomes

$$\int d^4x\, S(x,k) = \left(2\pi R^2\right)^{3/2} \sum_s P_s \left[w_s \exp\left(\frac{\mathbf{k}\mathbf{u}_s}{T_s}\right) + w_s^* \exp\left(\frac{\mathbf{k}\mathbf{u}_s^*}{T_s}\right)\right], \tag{4.4}$$

while, the function $J(k, q)$ becomes

$$J(k,q) = Q_c \sum_s Q_s \left[w_s \exp\left[\left(\mathbf{k}+\frac{\mathbf{q}}{2}\right)\frac{\mathbf{u}_s}{T_s}\right] e^{i\mathbf{q}\mathbf{x}_s} + w_s^* \exp\left[\left(\mathbf{k}+\frac{\mathbf{q}}{2}\right)\frac{\mathbf{u}_s^*}{T_s}\right] e^{i\mathbf{q}\mathbf{x}_s^*}\right] \tag{4.5}$$

Only the mirror symmetry across the reaction plane is assumed, which is always true for globally symmetric, A+A, heavy ion collisions in a non-fluctuating fluid dynamical model calculation. Then the correlation function can be evaluated using eqs. (1.26) and (1.29). (See the APPENDIX for further details.)

4.2 The Freeze-out Weights

While the flow symmetries discussed above depend on the initial collision symmetries, the weights do not follow these. The ansatz used earlier leads

the weights as given in Eq. (4.3). These weights depend on the local mean emission direction $\hat{\sigma}^\mu$, the flow velocity at the emission point and the opacity along the integrated path of the propagation of the emitted particle along this direction. The emission probability from different points of the space time is discussed in more detail earlier which was based primarily on Refs. [18, 19]. These considerations may be more involved than the ansatz taken over from [21]. The determination of the FO surface normal or the mean emission direction from the ST freeze-out layer and the emission profile in this layer are the subjects of present theoretical research, see [39, 40, 41, 42]. Here we do not discuss the effect of opacity along the path of the emission.

The detector configuration is given by the two particles reaching a given detector in the direction of $\mathbf{k}$. Thus the emission weights depend on the direction of the normal of the emission surface and of the emission, i.e. $\hat{\sigma}$ and $\hat{k}$. Furthermore, most monte-carlo cascade type of studies indicate [39, 40, 43], that the majority of particles freezes out in a layer along a constant proper time hyperbola, with a dominant flow 4-velocity, which is normal to this hyperbola: $\hat{\sigma}^\mu \approx u^\mu$. The origin of the hyperbola is at a ST point, which at low beam energies precedes the impact of the Lorentz contracted nuclei [39].

We assume in the actual numerical calculations that in the expression of the weight, Eq. (4.3), $Q_s(q)$ is the same for all surface layer elements: $Q_s^{(q)} = Q^{(q)}$ and $\Theta_s = \Theta$, so that $w_s = (k_\mu\, \hat{\sigma}_s^\mu)\ \exp(-\Theta^2 q_0^2/2)$, where $\hat{\sigma}_{s\mu} = (\sigma_s^0, \sigma_s)$, so that $k_\mu\, \hat{\sigma}_s^\mu = k^0\sigma_s^0 + \mathbf{k}\sigma_s$. If emission path time-length, Θ, tends to zero, then the time modifying factor becomes unity. With the choice $\hat{\sigma}_\mu = u_\mu$, the time-like FO normal is $\hat{\sigma}_{s\mu} = (\gamma_s, \mathbf{u}_s)$. Then $(k_\mu \hat{\sigma}_s^\mu) = \gamma_s k_0 + \mathbf{k}\mathbf{u}_s$. So the weight becomes

$$w_s = (\gamma_s k_0 + \mathbf{k}\mathbf{u}_s)\ \exp(-\Theta^2 q_0^2/2). \tag{4.6}$$

This weight is explicitly different for the mirror image cell at $\mathbf{x}_s^* \to -\mathbf{x}_s$, where $\mathbf{u}_s^* \to -\mathbf{u}_s$ and then $w_s^* = (\gamma_s k_0 - \mathbf{k}\mathbf{u}_s) \exp(-\Theta^2 q_0^2/2)$.

The weight factors appear both in the nominator and denominator of the correlator, so its normalization is balanced. On the other hand the role of the different factors in the weight have an effect to determine which cells contribute more or less to the result. This is a fundamental problem of the FO process, and in real situations it can get further convoluted if the hadronization and FO coincide in a rapid expansion.

4.3 Results

The sensitivity of the standard correlation function on the fluid cell velocities decreases with decreasing distances among the cells. So, with a large number of densely places fluid cells where all fluid cells contribute equally to the correlation function, the sensitivity on the flow velocity becomes negligibly weak.

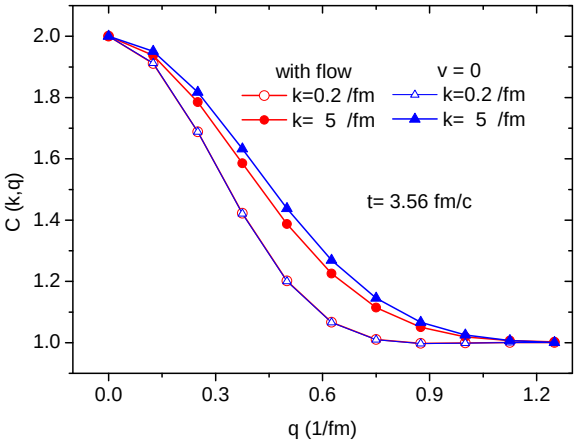

Figure 4.1: (color online) The dependence of the standard correlation function in the $\mathbf{k}_+$ direction from the collective flow, at the final time.

Thus, the emission probability from different ST regions of the system is essential in the evaluation. This emission asymmetry due to the local flow velocity occurs also when the FO surface or layer is isochronous or if it happens at constant proper time.

We studied the fluid dynamical patterns of the calculations published in Ref. [2], where the appearance of the KHI is discussed under different conditions. We chose the configuration, where both the rotation [1], and **the KHI occurred**, at $b = 0.7b_{max}$ with high cell resolution and low numerical viscosity at LHC energies, where the angular momentum is large, $L \approx 10^6\hbar$ [40].

We have used the Differential HBT method for simplified examples of a few fluid cells. These examples were spatially symmetric, thus the standard correlation function did not show any difference if it is measured at two symmetric $\mathbf{k}$ and $\mathbf{q}$-out angles, e.g. in the reaction, [x-z] plane at $\mathbf{k}_+ = (k_x, 0, +k_z)$ $\mathbf{q}_+ = (q_x, 0, +q_z)$ and $\mathbf{k}_- = (k_x, 0, -k_z)$ $\mathbf{q}_- = (q_x, 0, +q_-)$. Here

we have chosen two directions at $\eta = \pm 0.76$, that is at polar angles of 90 ± 40 degrees. These are measurable with the ALICE TPC detector and at the ATLAS and CMS detectors also.

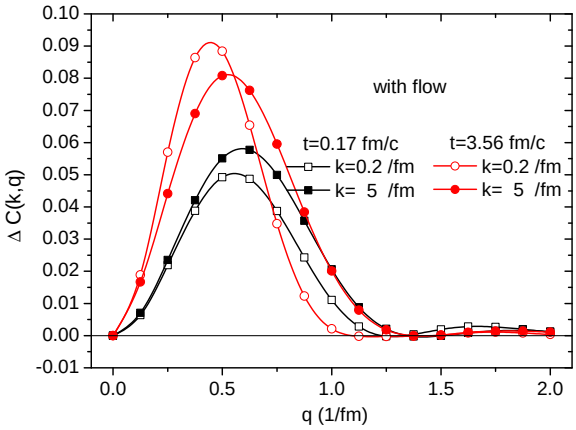

Figure 4.2: (color online) The differential correlation function $\Delta C(k, q)$ at the initial and final times of flow development.

The standard correlation function is both influenced by the ST shape of the emitting source as well as its velocity distribution. The correlation function becomes narrower in q with increasing time primarily due to the rapid expansion of the system. At the initial configuration the increase of $|\mathbf{k}|$ leads to a small increase of the width of the correlation function

Nevertheless, in theoretical models we can switch of the flow, and analyse how the flow influences the correlation function and especially the differential correlation function, $\Delta C(k, q)$.

Fig. 4.1 compares the standard correlation functions with and without the collective flow at the final time moment. Here we see that the flow causes a decrease of the width in q for the distribution at high values of $|\mathbf{k}|$.

The differential correlation function is more sensitive on the flow as it is shown in the few source models. In Fig. 4.2 $\Delta C(k, q)$ is shown for the initial and final times. Although the amplitude of the differential correlation function is smaller the differences between the initial and final configurations are significant. The dependence on $|\mathbf{k}|$ is especially large at the final time.

At the final time the flow dependence is again minimal at small momenta, $|\mathbf{k}|$, while at large momenta the flow leads to a change in the shape of the differential correlation function, and leads to an increase of its amplitude,

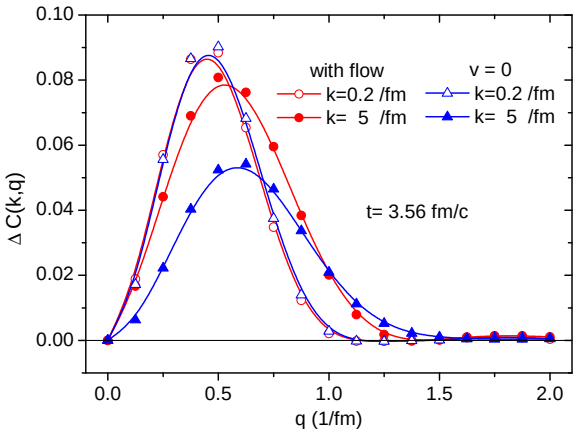

Figure 4.3: (color online) The flow velocity dependence of the differential correlation function at the final time.

Fig. 4.3. Here the expansion and the flow interfere with each other and this leads to a more complex behaviour.

These tests demonstrate that the differential correlation function is sensitive to the flow and its rotation.

4.4 Differential HBT and Separation of Shape effects

The original description was to measure $C(k, q_{out})$ [or $C(k, q_{long})$] in the reaction, $(x.z)$ plane at two different k directions around k_x shifted symmetrically forward and backward in the z-direction: $k+$ and $k-$. Then if the emitting object is symmetric for $\pm z$, and the object does not rotate then $\Delta C \equiv C(k+, q_{out}) - C(k-, q_{out})$ vanishes, but if there is a rotation then ΔC does not vanish. This is also true if the flow velocity pattern is also symmetric for $\pm z$, e.g. for spherical expansion. But not for rotation!

In general the problem is that the emitting object is neither spherical nor symmetric over $\pm z$ reflection in most realistic situations. In this case the method becomes problematic because both the rotation and the shape asymmetry over $\pm z$, will lead to non-vanishing ΔC.

Therefore our aim is to separate the (i) rotation effect and (ii) the shape and spherical flow effect on the two particle correlations.

The symmetry axes, for the case (ii) were determined and analysed by the azimuth-dependent HBT method in refs. [8], and it was found that the source can be approximated well as a three axis ellipsoid, where two of the axes are in the reaction plane and the third in the transverse plane. The major axis in the reaction plane is correlated with the directed flow with a well identified tilt-angle, while the dominant expansion happened in the orthogonal direction, creating the "anti-flow" or "third flow component" [44, 45]. If we perform a reflection of the source across one of these two axis in the reaction plane, we get an almost identical mirror image configuration, except that the rotation will be reversed. Let us denote the axis, which is orthogonal to the major tilt-axis as the x'-axis. The polar angle of this axis is the tilt-axis plus 90 degrees: $\Theta_s + \pi/2$, i.e. 137, 127, 123 degrees for the three cases at energies 2, 4, 6 GeV/nucl. respectively for the cases discussed in ref. [8].

Thus, if the original source was

$$S(x, y, z)\,,$$

and the reflected source is : $REF\{S(x, y, z)\}$, which is thus (almost) identical except rotation, then the combination:

$$S_0(x, y, z) \equiv [S(x, y, z) + REF\{S(x, y, z)\}]/2\,,$$

(a) will have (almost) identical shape and radial flow distribution as the original source distribution, (b) will be exactly symmetric for reflection over the x'-axis, (c) will have vanishing rotation, and (d) will have vanishing $\Delta C(k_{x'}, q_{out})$ for two shifted $k+$ and $k-$ values with respect to the $k_{x'}$-axis.

Comparing this $\Delta C(k_{x'}, q_{out})$ for the S_0-distribution, with the $\Delta C(k_{x'}, q_{out})$ for the original S-distribution will give a good and quite precise measure for the average rotation of the original distribution.

Chapter 5

Conclusions

In this work we attempted to study the possibility of detecting and evaluating the rotation of a source by the specific use of the Hanbury Brown and Twiss method for rotating systems. Our primary interest was the application for ultra-relativistic heavy ions where in peripheral collisions at ultra-relativistic energies the system can gain large angular momentum. Nevertheless, some of the conclusions can be applied to macroscopic systems also, like for fast rotating binary stars.

We selected one of the several methods to evaluate two particle correlations, which was suitable to study collective fluid systems with significant and well defined internal fluid dynamical motion. The obtained standard correlation functions were showing the consequences of the flow, but for highly symmetric sources the correlation functions gave symmetric results, which were invariant for the change of the direction of rotation.

It turned out that it is important to take into account that the particles reaching the detector cannot reach it with equal probability from the near side and the far side of the emitting object. With this fact considered we could obtain correlation functions, which reflected the properties and also the direction of the flow. These results can be used rather generally.

The obtained results has shown that the correlation function is most sensitive to the rotation if it is measured in the beam direction (or close to it). This, unfortunately, is not possible in most heavy ion accelerator experiments, so we introduced and investigated a Differential Hanbury Brown and Twiss method, which made it possible to trace down the rotation in relativistic heavy ion collisions by measuring the correlation functions in the reaction plane at nearly transverse angles to the beam direction. The method

is promising and can be performed in most heavy ion experiments without difficulties, as well as it can be implemented in different reaction models, like fluid dynamical models, microscopic transport models and hybrid models. In full scale theoretical models, the emission probabilities from the FO layer have to be considered. From the general formulas derived in the beginning of the paper apparently these dependencies can be factorized.

The present initial studies verify the dependence of the differential correlation function on the flow in general. At the same time it also shows that in realistic model situations the effect of the spatial size and shape, the flow expansion and the flow rotation all influence the differential correlation function. In the Differential HBT analysis one can disentangle the effect of rotation from the effects of shape and radial flow.

Exploiting the results of azimuth-dependent HBT analysis and the arising symmetry axes provided by this analysis [8], one can generate, with a reflection of the source distribution, another source with almost identical shape, that is exactly symmetric with respect to one of the given symmetry axes, but which has no rotation. The source generated this way provides vanishing ΔC, and thus it provides a good quantitative measure for the rotation by performing the differential HBT analysis in the same reference frame for the original source distribution.

In addition theoretical model studies should be complemented with experimental investigations. In this case it is important to determine the precise Event by Event c.m. position of the participants [27], and minimize the effect of fluctuations to be able to measure accurately the emission angles, which are crucial in the present $\Delta C(k, q)$ studies.

Chapter 6

APPENDIX

6.1 Appendix A - Four Symmetric Sources

Correlation function for a pair of two sources.

From equations (1.26) and (1.29) we can derive the correlation function for a pair of two sources.

$J(k,q)$ is defined in equation (1.28) so we have

$$J(k,q) = E_k \left(2\pi R^2\right)^{3/2} \exp\left(-\frac{R^2q^2}{2}\right) \sum_s \frac{n_s}{C_s} \exp\left[-\frac{k\cdot u_s}{T_s}\right] \exp\left[-\frac{q\cdot u_s}{2T_s}\right] \exp(iqx_s) =$$

$$E_k \left(2\pi R^2\right)^{3/2} \exp\left(-\frac{R^2}{2}q^2\right) \frac{n_s}{C_s} \exp\left[-\frac{k^0\gamma_s}{T_s}\right] \exp\left[-\frac{q^0}{2}\frac{\gamma_s}{T_s}\right] \exp(iq^0x_s^0)\times$$

$$\left[\exp\left[\frac{\mathbf{k}\cdot\mathbf{u}_{s_1}}{T_s}\right] \exp\left[\frac{\mathbf{q}\cdot\mathbf{u}_{s_1}}{2T_s}\right] \exp(i\mathbf{q}\cdot\mathbf{x}_{s_1}) + \exp\left[-\frac{\mathbf{k}\cdot\mathbf{u}_{s_1}}{T_s}\right] \exp\left[-\frac{\mathbf{q}\cdot\mathbf{u}_{s_1}}{2T_s}\right] \exp(-i\mathbf{q}\cdot\mathbf{x}_{s_1}) + \right.$$

$$\left. \exp\left[\frac{\mathbf{k}\cdot\mathbf{u}_{s_2}}{T_s}\right] \exp\left[\frac{\mathbf{q}\cdot\mathbf{u}_{s_2}}{2T_s}\right] \exp(i\mathbf{q}\cdot\mathbf{x}_{s_2}) + \exp\left[-\frac{\mathbf{k}\cdot\mathbf{u}_{s_2}}{T_s}\right] \exp\left[-\frac{\mathbf{q}\cdot\mathbf{u}_{s_2}}{2T_s}\right] \exp(-i\mathbf{q}\cdot\mathbf{x}_{s_2})\right] \tag{6.1}$$

and for the denominator:

$$\int d^3x\ S(x,k) = \sum_s \int_S d^4x\ S_s(x,k) = E_k\ \left(2\pi R^2\right)^{3/2} \sum_s \frac{n_s}{C_s} \exp\left[-\frac{k\cdot u_s}{T_s}\right] = E_k\ \left(2\pi R^2\right)^{3/2} \frac{n_s}{C_s} \exp\left[-\frac{k^0\gamma_s}{T_s}\right] \times \left(\exp\left[\frac{\mathbf{k}\cdot\mathbf{u}_{s_1}}{T_s}\right] + \exp\left[-\frac{\mathbf{k}\cdot\mathbf{u}_{s_1}}{T_s}\right] + \exp\left[\frac{\mathbf{k}\cdot\mathbf{u}_{s_2}}{T_s}\right] + \exp\left[-\frac{\mathbf{k}\cdot\mathbf{u}_{s_2}}{T_s}\right]\right) \tag{6.2}$$

By using (1.26) and (1.29) we are left with only exponential functions. We use the same result as in equation (2.22) for exponentials products with only s_1 or s_2. The real value gives

$$Re[\,exp\,(\pm i\mathbf{q}\cdot(\mathbf{x}_{s_1}\pm\mathbf{x}_{s_2})] = cos\,(\mathbf{q}\cdot(\mathbf{x}_{s_1}\pm\mathbf{x}_{s_2})) \tag{6.3}$$

In the numerator we will have after taking the product J(k,q)J(k,-q) the terms

$$\begin{aligned}
&\left[\exp\left(\frac{2\mathbf{k}\cdot\mathbf{u}_{s_1}-\mathbf{q}\cdot\mathbf{u}_{s_1}-2\mathbf{k}\cdot\mathbf{u}_{s_2}-\mathbf{q}\cdot\mathbf{u}_{s_2}}{2T_s}\right)+\right.\\
&\left.\exp\left(\frac{-2\mathbf{k}\cdot\mathbf{u}_{s_1}+\mathbf{q}\cdot\mathbf{u}_{s_1}+2\mathbf{k}\cdot\mathbf{u}_{s_2}+\mathbf{q}\cdot\mathbf{u}_{s_2}}{2T_s}\right)\right]\cos(\mathbf{q}\cdot(\mathbf{x}_{s_1}+\mathbf{x}_{s_2}))+\\
&\left[exp\left(\frac{2\mathbf{k}\cdot\mathbf{u}_{s_1}+\mathbf{q}\cdot\mathbf{u}_{s_1}-2\mathbf{k}\cdot\mathbf{u}_{s_2}+\mathbf{q}\cdot\mathbf{u}_{s_2}}{2T_s}\right)+\right.\\
&\left.exp\left(\frac{-2\mathbf{k}\cdot\mathbf{u}_{s_1}-\mathbf{q}\cdot\mathbf{u}_{s_1}+2\mathbf{k}\cdot\mathbf{u}_{s_2}-\mathbf{q}\cdot\mathbf{u}_{s_2}}{2T_s}\right)\right]\cos(\mathbf{q}\cdot(\mathbf{x}_{s_1}+\mathbf{x}_{s_2}))+\\
&\left[exp\left(\frac{2\mathbf{k}\cdot\mathbf{u}_{s_1}-\mathbf{q}\cdot\mathbf{u}_{s_1}+2\mathbf{k}\cdot\mathbf{u}_{s_2}+\mathbf{q}\cdot\mathbf{u}_{s_2}}{2T_s}\right)+\right.\\
&\left.exp\left(\frac{-2\mathbf{k}\cdot\mathbf{u}_{s_1}+\mathbf{q}\cdot\mathbf{u}_{s_1}-2\mathbf{k}\cdot\mathbf{u}_{s_2}-\mathbf{q}\cdot\mathbf{u}_{s_2}}{2T_s}\right)\right]\cos(\mathbf{q}\cdot(\mathbf{x}_{s_1}-\mathbf{x}_{s_2}))+\\
&\left[exp\left(\frac{2\mathbf{k}\cdot\mathbf{u}_{s_1}+\mathbf{q}\cdot\mathbf{u}_{s_1}+2\mathbf{k}\cdot\mathbf{u}_{s_2}-\mathbf{q}\cdot\mathbf{u}_{s_2}}{2T_s}\right)+\right.\\
&\left.exp\left(\frac{-2\mathbf{k}\cdot\mathbf{u}_{s_1}-\mathbf{q}\cdot\mathbf{u}_{s_1}-2\mathbf{k}\cdot\mathbf{u}_{s_2}+\mathbf{q}\cdot\mathbf{u}_{s_2}}{2T_s}\right)\right]\cos(\mathbf{q}\cdot(\mathbf{x}_{s_1}-\mathbf{x}_{s_2}))\ .
\end{aligned} \tag{6.4}$$

We will then use the following relation:

$$\exp(a+b)+\exp(a-b)+\exp(-a+b)+\exp(-a-b) = 4\cosh(a)\cosh(b) \quad (6.5)$$

This will give equation (2.28) after taking the square of the denominator which is done similarly.

6.2 Appendix B - Four sources with asymmetric emission

The out component of the four source correlation function with $a = b$, $d_x = d_z$ and $v_x = v_z$. We will use $\frac{\gamma v_x a}{T_s} = \frac{\gamma v_x b}{T_s} = A$ and $ad_x = bd_z = B$. So equation (3.11) becomes

$$\begin{aligned}
&C(k_{(\pm)}, q_{out}) = 1 + \exp(-R^2q^2)\ [2\omega_a\omega_b + 2\omega_c\omega_d + \\
&\omega_a^2 \exp(\pm 2Ak) \exp(\pm Ak) \cos(2Bq) + \omega_b^2 \exp(\mp 2Ak) \exp(\mp Ak) \cos(2Bq) + \\
&\omega_c^2 \exp(2Ak) \exp(Ak) \cos(2Bq) + \omega_d^2 \exp(-2Ak) \exp(-Ak) \cos(2Bq) + \\
&2\omega_a\omega_c \exp(\pm Ak) \exp\left(\pm\frac{Ak}{2}\right) \exp(Ak) \exp\left(\frac{Ak}{2}\right) \cos((B \pm B)q) + \\
&2\omega_b\omega_d \exp(\mp Ak) \exp\left(\mp\frac{Ak}{2}\right) \exp(-Ak) \exp\left(-\frac{Ak}{2}\right) \cos((B \pm B)q) + \\
&2\omega_a\omega_d \exp(\pm Ak) \exp\left(\pm\frac{Ak}{2}\right) \exp(-Ak) \exp\left(-\frac{Ak}{2}\right) \cos((B \mp B)q) + \\
&2\omega_b\omega_c \exp(\mp Ak) \exp\left(\mp\frac{Ak}{2}\right) \exp(Ak) \exp\left(\frac{Ak}{2}\right) \cos((B \mp B)q)\Big] \times \\
&[\omega_a \exp(\pm Ak) + \omega_b \exp(\mp Ak) + \omega_c \exp(Ak) + \omega_d \exp(-Ak)]^{-2} \ .
\end{aligned} \quad (6.6)$$

For the difference we then have

$$\begin{aligned}
&\Delta(k_{\pm}, q_{out}) \equiv C(k_+, q_{out}) - C(k_-, q_{out}) = \\
&exp(-R^2q^2) \times [2\omega_a\omega_b + 2\omega_c\omega_d + 2\omega_a\omega_d + 2\omega_b\omega_c + \\
&(\omega_a^2 + \omega_c^2 + 2\omega_a\omega_c)\exp(2Ak)\exp(Ak)\cos(2Bq) + \\
&(\omega_b^2 + \omega_d^2 + 2\omega_b\omega_d)\exp(-2Ak)\exp(-Ak)\cos(2Bq)\ ] \\
&[(\omega_a + \omega_c)\exp(Ak) + (\omega_b + \omega_d)\exp(-Ak)]^{-1} - \\
&exp(-R^2q^2) \times \Big[2\omega_a^{'}\omega_b^{'} + 2\omega_c^{'}\omega_d^{'} + 2\omega_a^{'}\omega_c^{'} + 2\omega_b^{'}\omega_d^{'} + \\
&(\omega_b^{'2} + \omega_c^{'2} + 2\omega_b^{'}\omega_c^{'})\exp(2Ak)\exp(Ak)\cos(2Bq) + \\
&(\omega_a^{'2} + \omega_d^{'2} + 2\omega_a^{'}\omega_d^{'})\exp(-2Ak)\exp(-Ak)\cos(2Bq)\ \Big] \\
&\Big[(\omega_b^{'} + \omega_c^{'})\exp(Ak) + (\omega_a^{'} + \omega_d^{'})\exp(-Ak)\Big]^{-1}
\end{aligned} \tag{6.7}$$

where for figures (3.4) and (3.5) we would have $\omega_a^{'} = \omega_a$, $\omega_b^{'} = \omega_b$, $\omega_c^{'} = \omega_d$, $\omega_d^{'} = \omega_c$

6.3 Appendix C - The CFD cell structure

The fluid cells are spatially cubic, the axes and the edges of the cubes are parallel, and the axes are situated at the lines of the edges of the 1st row of cells in every direction. Thus, the centers of the 1st layer of cells are at a distance of $\frac{1}{2}d$, where d is the cell-size in each spatial direction.

Due to the symmetries of the pre-collision initial state the system is mirror symmetric with respect to the $[x, z]$, reaction plane. Thus, it is sufficient to describe the cells on the positive side of the y-axis, because the other side is the mirror image of the positive side. Cell are labeled with indexes i, j, k in the x, y, z directions where the centers of a cell labeled by i, j, k are at the points:

$$\mathbf{x}_{ijk} = \left((i - i_{mid} - \frac{1}{2})d,\ (j - \frac{1}{2})d,\ (k - k_{mid} - \frac{1}{2})d\right), \tag{6.8}$$

where $i = i_{min}, i_{min}+1, i_{min}+2, \ldots\ i_{max}$, $j = 1, 2, 3, \ldots\ j_{max}$, and $k = k_{min}, k_{min}+1, k_{min}+2, \ldots\ k_{max}$, so that we do not calculate and store the cells at negative y-values, (j-values). The center of mass, as well as the

center of our calculation frame at $\mathbf{x} = (0, 0, 0)$ is between the cells indexed by $(i_{mid}, i_{mid}{+}1)$ and $(k_{mid}, k_{mid}{+}1)$, for x and z, while for y it is at the side of the $j = 1$ cells. The choice is such that $i_{min} > 0$ and $k_{min} > 0$. Thus, in this counting there are no cells with zero or negative indexes. At the same time these cells should be doubled and the negative y- side should also be counted for the evaluation of measurable quantities like two particle correlation characteristics. The cell parameters for the negative y-side cells, for invariant scalar quantities, q, and for 4-vector components are given as

$$\begin{aligned} q(-x,-y,-z) &= q(x,y,z) \\ \gamma_s(-x,-y,-z) &= \gamma_s(x,y,z) \\ v_x(-x,-y,-z) &= -v_x(x,y,z) \\ v_y(-x,-y,-z) &= -v_y(x,y,z) \\ v_z(-x,-y,-z) &= -v_z(x,y,z) \end{aligned} \tag{6.9}$$

where $u_s^\mu = \gamma_s(1, v_x, v_y, v_z)$ are the coordinates of the 4-velocity and $\mathbf{v}_s = (v_x, v_y, v_z)$. In the x, y and z directions if we have a cell with indexes (i, j, k) the corresponding mirror image cell has the indexes (i, j, k) $\longrightarrow$ ($2i_{mid}{-}i{+}1$, $-j$, $2k_{mid}{-}k{+}1$).

6.4 Appendix D - Correlation function for 2 cells

Let us introduce the notation $\beta_s \equiv \mathbf{u}_s/T_s$, and consider one cell at $j = 1$ with its mirror image cell at $j = -1$. The two cells are bordered to the origo at the corner of the cells. All scalar parameters are equal for the two cells. The cell in the top layer ($x > 0$) have velocity parameter β_s, while for the bottom layer $-\beta_s$. The positions of the cell centers are $(\pm x_s, \pm y_s, \pm z_s)$. The weights are not necessarily the same: $w_s(j > 0) \neq w_s^*(j < 0)$.

Then the function $S(k, q)$ becomes

$$\int d^4x\, S(x,k) = \left(2\pi R^2\right)^{3/2} P_s \left[w_s \exp\left(\mathbf{k}\beta_s\right) + w_s^* \exp\left(-\mathbf{k}\beta_s\right)\right]. \tag{6.10}$$

The denominator is then

$$\left|\int d^4x\, S(x,k)\right|^2 = \left(2\pi R^2\right)^3 P_s^2 \left[w_s^2 \exp\left(2\mathbf{k}\beta_s\right) + \left(w_s^*\right)^2 \exp\left(-2\mathbf{k}\beta_s\right) + 2w_s w_s^*\right]. \tag{6.11}$$

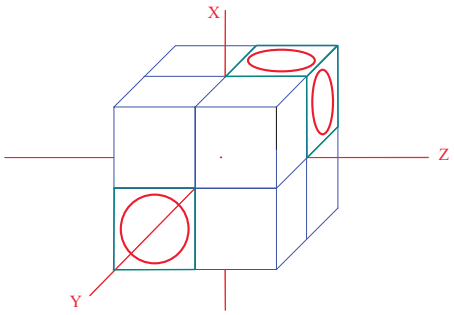

Figure 6.1: (color online) Two indicated fluid cells, placed symmetrically around the origin of the Descartes coordinate system. The cells on the negative y-side of the coordinate space (further away from us) are reflected around the point of origin (c.m.) and are not calculated explicitly in the fluid dynamical model. The velocity of the two cells point to the opposite directions.

Similarly the function $J(k,q)$ becomes

$$J(k,q) = \; Q_c P_s Q_s^q \left[w_s e^{\mathbf{k}\beta_s} \, e^{\mathbf{q}\beta_s/2} e^{i\mathbf{q}\mathbf{x}_s} + w_s^* e^{-\mathbf{k}\beta_s} \, e^{-\mathbf{q}\beta_s/2} e^{-i\mathbf{q}\mathbf{x}_s} \right] \; , \qquad (6.12)$$

where $\mathbf{x}_s$ is the position of the center of the cell on the positive y side, while the mirror image cell has $-\mathbf{x}_s$. Let us introduce the notations:

$$\Sigma(\mathbf{q}) = e^{i\mathbf{q}\mathbf{x}_s}. \qquad (6.13)$$

Then in the above expression we can insert $e^{i\mathbf{q}\mathbf{x}_s} = \cos(\mathbf{q}\mathbf{x}_s) + i\sin(\mathbf{q}\mathbf{x}_s)$, so that

$$\Sigma(\mathbf{q}) = \; \cos \mathbf{q}\mathbf{x}_s + i \sin \mathbf{q}\mathbf{x}_s. \qquad (6.14)$$

Notice that $Re[\Sigma^2(\mathbf{q})] = Re[\Sigma^2(-\mathbf{q})] = C_q^2 - S_q^2$ and $Re[\Sigma(\mathbf{q})\Sigma(-\mathbf{q})] = C_q^2 + S_q^2$, where $C_q = \cos \mathbf{q}\mathbf{x}_s$, and $S_q = \sin \mathbf{q}\mathbf{x}_s$.

Using this substitution the $Re[J(k,q)J(k,-q)]$ product becomes:

$$
\begin{aligned}
&Re[J(k,q)J(k,-q)] = \\
&(Q_c P_s)^2 Re\left[\left(w_s e^{\mathbf{k}\beta_s} e^{\mathbf{q}\beta_s/2}\Sigma(\mathbf{q}) + w_s^* e^{-\mathbf{k}\beta_s} e^{-\mathbf{q}\beta_s/2}\Sigma(-\mathbf{q})\right) \times\right. \\
&\left.\left(w_s e^{\mathbf{k}\beta_s} e^{-\mathbf{q}\beta_s/2}\Sigma(-\mathbf{q}) + w_s^* e^{-\mathbf{k}\beta_s} e^{\mathbf{q}\beta_s/2}\Sigma(\mathbf{q})\right)\right] = \\
&(Q_c P_s)^2 Re\left[w_s^2 e^{\mathbf{k}\beta_s} e^{\mathbf{q}\beta_s/2}\ e^{\mathbf{k}\beta_s} e^{-\mathbf{q}\beta_s/2}\ \Sigma(\mathbf{q})\Sigma(-\mathbf{q}) + w_s\, w_s^*\, e^{\mathbf{k}\beta_s} e^{\mathbf{q}\beta_s/2}\ e^{-\mathbf{k}\beta_s} e^{\mathbf{q}\beta_s/2}\ \Sigma^2(\mathbf{q}) + \right. \\
&\left. w_s^*\, w_s\, e^{-\mathbf{k}\beta_s} e^{-\mathbf{q}\beta_s/2}\ e^{\mathbf{k}\beta_s} e^{-\mathbf{q}\beta_s/2}\ \Sigma^2(-\mathbf{q}) + (w_s^*)^2 e^{-\mathbf{k}\beta_s} e^{-\mathbf{q}\beta_s/2}\ e^{-\mathbf{k}\beta_s} e^{\mathbf{q}\beta_s/2}\ \Sigma(-\mathbf{q})\Sigma(\mathbf{q})\right] = \\
&(Q_c P_s)^2 Re\left[w_s^2 e^{2\mathbf{k}\beta_s}\ \Sigma(\mathbf{q})\Sigma(-\mathbf{q}) + w_s\, w_s^*\, e^{\mathbf{q}\beta_s}\ \Sigma^2(\mathbf{q}) + \right. \\
&\left. w_s\, w_s^*\, e^{-\mathbf{q}\beta_s}\ \Sigma^2(-\mathbf{q}) + (w_s^*)^2\, e^{-2\mathbf{k}\beta_s}\ \Sigma(-\mathbf{q})\Sigma(\mathbf{q})\right] = \\
&(Q_c P_s)^2\left[2\, w_s\, w_s^*\ \cosh(\mathbf{q}\beta_s)\,(C_q^2 - S_q^2) + \left[w_s^2 e^{2\mathbf{k}\beta_s} + (w_s^*)^2 e^{-2\mathbf{k}\beta_s}\right]\ (C_q^2 + S_q^2)\right]
\end{aligned}
$$

Here we exploited the fact that in the product $J(k,q)\,J(k,-q)$ the factor $Q_s^q\, Q_s^{-q}$ reduces to unity.

Thus the correlation function becomes:

$$
\begin{aligned}
C(k,q) =& 1 + \exp(-R^2 q^2)\times \\
&\frac{2\, w_s\, w_s^*\ \cosh(\mathbf{q}\beta_s)\,(C_q^2 - S_q^2) + \left[w_s^2 e^{2\mathbf{k}\beta_s} + (w_s^*)^2 e^{-2\mathbf{k}\beta_s}\right]\ (C_q^2 + S_q^2)}{w_s^2 \exp(2\mathbf{k}\beta_s) + (w_s^*)^2 \exp(-2\mathbf{k}\beta_s) + 2 w_s w_s^*}
\end{aligned}
\tag{6.15}
$$

Due to the symmetric configuration the coefficients $(C_q^2 + S_q^2)$ and $(C_q^2 - S_q^2)$ could be simplified further.

6.5 Appendix E - Correlation function for 8 cells

Let us introduce the notation $\beta_s \equiv \mathbf{u}_s/T_s$, and consider 4 cells at $j = 1$ with 4 mirror image cells at $j = -1$. In this example we assume that all top/bottom-layer cells have the same velocity and temperature, which is in general not the case. The 8 cells form a tight cube enclosing the origo at the corner of the inside cell boundaries. All scalar parameters are equal for all cells. All cells of the top layer ($x > 0$) have the same velocity parameter β, while for the

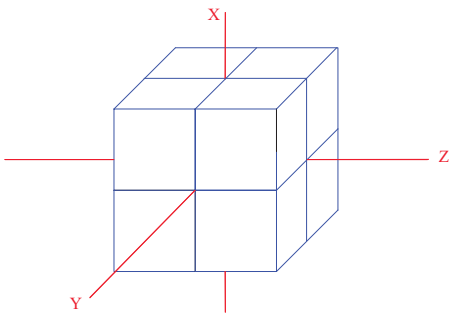

Figure 6.2: (color online) Eight fluid cells, placed symmetrically around the origin of the Descartes coordinate system. The cells on the negative y-side of the coordinate space (further away from us) are reflected around the point of origin (c.m.) and are not calculated explicitly in the fluid dynamical model. The top layer has uniform velocity pointing to the right (positive z-direction), while the bottom layer has a uniform velocity to the opposite direction. Random fluctuations would violate this exact symmetry.

bottom layer $-\beta$. The positions of the cell centers are $(\pm x, \pm y, \pm z)$. Here all weights, (w_s and w_s^*) are the same, which is also not true in general.

Then the function $S(k,q)$ becomes

$$\int d^4x\, S(x,k) = \left(2\pi R^2\right)^{3/2} \sum_{s=1}^{4} P_s w_s \left[\exp\left(\mathbf{k}\beta\right) + \exp\left(-\mathbf{k}\beta\right)\right] =$$
$$4\left(2\pi R^2\right)^{3/2} P_s w_s \left[\exp\left(\mathbf{k}\beta\right) + \exp\left(-\mathbf{k}\beta\right)\right] = 8\left(2\pi R^2\right)^{3/2} P_s w_s \cosh\left(\mathbf{k}\beta\right) \tag{6.16}$$

The denominator is then

$$\left|\int d^4x\, S(x,k)\right|^2 = 64\left(2\pi R^2\right)^3 P_s^2 w_s^2 \cosh(2\mathbf{k}\beta)\ . \tag{6.17}$$

Similarly the function $J(k,q)$ becomes

$$J(k,q) = Q_c \sum_{s=1}^{4} P_s \left[Q_s^q w_s \exp\left[\left(\mathbf{k}+\frac{\mathbf{q}}{2}\right)\frac{\mathbf{u}_s}{T_s} \right] e^{i\mathbf{q}\mathbf{x}_s} Q_s^q w_s^* \exp\left[\left(\mathbf{k}+\frac{\mathbf{q}}{2}\right)\frac{\mathbf{u}_s^*}{T_s} \right] e^{i\mathbf{q}\mathbf{x}_s^*} \right] =$$

$$Q_c P_s Q_s^q w_s \left\{ e^{\mathbf{k}\beta} e^{\mathbf{q}\beta/2} \left[e^{i\mathbf{q}\mathbf{x}_a} + e^{i\mathbf{q}\mathbf{x}_b} + e^{i\mathbf{q}\mathbf{x}_c} + e^{i\mathbf{q}\mathbf{x}_d} \right] + e^{-\mathbf{k}\beta} e^{-\mathbf{q}\beta/2} \left[e^{-i\mathbf{q}\mathbf{x}_a} + e^{-i\mathbf{q}\mathbf{x}_b} + e^{-i\mathbf{q}\mathbf{x}_c} + e^{-i\mathbf{q}\mathbf{x}_d} \right] \right\} ,$$

where $\mathbf{x}_a$, $\mathbf{x}_b$, $\mathbf{x}_c$, $\mathbf{x}_d$ are the positions of the centers of the 4 cells in the top layer, while the bottom layer has the mirror image cells. Let us introduce the notations:

$$\Sigma(\mathbf{q}) = e^{i\mathbf{q}\mathbf{x}_a} + e^{i\mathbf{q}\mathbf{x}_b} + e^{i\mathbf{q}\mathbf{x}_c} + e^{i\mathbf{q}\mathbf{x}_d} \tag{6.18}$$

Then in the above expression we can insert for all 8 cells $e^{i\mathbf{q}\mathbf{x}_g} = \cos(\mathbf{q}\mathbf{x}_g) + i\sin(\mathbf{q}\mathbf{x}_g)$.

$$\begin{aligned} \Sigma(\mathbf{q}) = {} & \cos\mathbf{q}\mathbf{x}_a + \cos\mathbf{q}\mathbf{x}_b + \cos\mathbf{q}\mathbf{x}_c + \cos\mathbf{q}\mathbf{x}_d + \\ & i\left[\sin\mathbf{q}\mathbf{x}_a + \sin\mathbf{q}\mathbf{x}_b + \sin\mathbf{q}\mathbf{x}_c + \sin\mathbf{q}\mathbf{x}_d\right]. \end{aligned} \tag{6.19}$$

Notice that $Re[\Sigma^2(\mathbf{q})] = Re[\Sigma^2(-\mathbf{q})] = C_q^2 - S_q^2$ and
$Re[\Sigma(\mathbf{q})\Sigma(-\mathbf{q})] = C_q^2 + S_q^2$, where
$C_q = \cos\mathbf{q}\mathbf{x}_a + \cos\mathbf{q}\mathbf{x}_b + \cos\mathbf{q}\mathbf{x}_c + \cos\mathbf{q}\mathbf{x}_d$, and
$S_q = \sin\mathbf{q}\mathbf{x}_a + \sin\mathbf{q}\mathbf{x}_b + \sin\mathbf{q}\mathbf{x}_c + \sin\mathbf{q}\mathbf{x}_d$.

Using this substitution the $Re[J(k,q)J(k,-q)]$ product becomes:

$$\begin{aligned} & Re[J(k,q)J(k,-q)] = \\ & (Q_c P_s w_s)^2 Re\left[\left(e^{\mathbf{k}\beta} e^{\mathbf{q}\beta/2}\Sigma(\mathbf{q}) + e^{-\mathbf{k}\beta} e^{-\mathbf{q}\beta/2}\Sigma(-\mathbf{q})\right)\left(e^{\mathbf{k}\beta} e^{-\mathbf{q}\beta/2}\Sigma(-\mathbf{q}) + e^{-\mathbf{k}\beta} e^{\mathbf{q}\beta/2}\Sigma(\mathbf{q})\right)\right] = \\ & (Q_c P_s w_s)^2 Re\left[e^{\mathbf{k}\beta} e^{\mathbf{q}\beta/2}\ e^{\mathbf{k}\beta} e^{-\mathbf{q}\beta/2}\ \Sigma(\mathbf{q})\Sigma(-\mathbf{q}) + e^{\mathbf{k}\beta} e^{\mathbf{q}\beta/2}\ e^{-\mathbf{k}\beta} e^{\mathbf{q}\beta/2}\ \Sigma^2(\mathbf{q}) + \right. \\ & \left. e^{-\mathbf{k}\beta} e^{-\mathbf{q}\beta/2}\ e^{\mathbf{k}\beta} e^{-\mathbf{q}\beta/2}\ \Sigma^2(-\mathbf{q}) + e^{-\mathbf{k}\beta} e^{-\mathbf{q}\beta/2}\ e^{-\mathbf{k}\beta} e^{\mathbf{q}\beta/2}\ \Sigma(-\mathbf{q})\Sigma(\mathbf{q})\right] = \\ & (Q_c P_s w_s)^2 Re\left[e^{2\mathbf{k}\beta}\ \Sigma(\mathbf{q})\Sigma(-\mathbf{q}) + e^{\mathbf{q}\beta}\ \Sigma^2(\mathbf{q}) + e^{-\mathbf{q}\beta}\ \Sigma^2(-\mathbf{q}) + e^{-2\mathbf{k}\beta}\ \Sigma(-\mathbf{q})\Sigma(\mathbf{q})\right] = \\ & 2\left(Q_c P_s w_s\right)^2 \left[\cosh(2\mathbf{k}\beta)(C_q^2 + S_q^2) + \cosh(\mathbf{q}\beta)(C_q^2 - S_q^2)\right] \end{aligned} \tag{6.20}$$

Here we exploited the fact that in the product $J(k,q)\,J(k,-q)$ the factor $Q_s^q\,Q_s^{-q}$ reduces to unity.

Thus the correlation function becomes:

$$C(k,q) = 1 + \exp(-R^2q^2)\frac{\left[\cosh(2\mathbf{k}\beta)(C_q^2 + S_q^2) + \cosh(\mathbf{q}\beta)(C_q^2 - S_q^2)\right]}{32\cosh(2\mathbf{k}\beta)} \tag{6.21}$$

Due to the symmetric configuration the coefficients $(C_q^2 + S_q^2)$ and $(C_q^2 - S_q^2)$ could be simplified further.

6.6 Appendix F - Correlation function for all cell-pairs

This is the general situation, only the mirror symmetry around the c.m. point of the participant assumed. This is generally true if we disregard random fluctuations.

Then the function $S(k,q)$ becomes

$$\int d^4x\, S(x,k) = \left(2\pi R^2\right)^{3/2} \sum_s P_s \mathcal{K}_s \ , \tag{6.22}$$

where

$$\mathcal{K}_s \equiv \left[w_s \exp\left(\mathbf{k}\beta_s\right) + w_s^* \exp\left(-\mathbf{k}\beta_s\right)\right] \ . \tag{6.23}$$

The denominator in the correlation function is then

$$\left|\int d^4x\, S(x,k)\right|^2 = \left(2\pi R^2\right)^3 \left[\sum_s P_s^2\, \mathcal{K}_s^2 + 2\sum_{s>s'} P_s P_{s'} \mathcal{K}_s \mathcal{K}_{s'}\right] \tag{6.24}$$

Similarly the function $J(k,q)$ becomes

$$J(k,q) = Q_c \sum_s P_s Q_s^{(q)} \left[w_s e^{(\mathbf{k}+\frac{\mathbf{q}}{2})\beta_s + i\mathbf{q}\mathbf{x}_s} + w_s^* e^{-(\mathbf{k}+\frac{\mathbf{q}}{2})\beta_s - i\mathbf{q}\mathbf{x}_s}\right].$$

Then in the above expression we can perform the substitution: $e^{i\mathbf{q}\mathbf{x}_s} = \cos(\mathbf{q}\mathbf{x}_s) + i\sin(\mathbf{q}\mathbf{x}_s)$, so the function $J(k,q)$ becomes

$$J(k,q) = Q_c \sum_s P_s Q_s^{(q)} \left[\mathcal{C}_s^{(q)} + i\,\mathcal{S}_s^{(q)}\right], \tag{6.25}$$

where $\mathcal{C}_s^{(q)} = \left[w_s e^{(\mathbf{k}+\frac{\mathbf{q}}{2})\beta_s} + w_s^* e^{-(\mathbf{k}+\frac{\mathbf{q}}{2})\beta_s}\right] \cos(\mathbf{q}\mathbf{x}_s)$ and
$\mathcal{S}_s^{(q)} = \left[w_s e^{(\mathbf{k}+\frac{\mathbf{q}}{2})\beta_s} - w_s^* e^{-(\mathbf{k}+\frac{\mathbf{q}}{2})\beta_s}\right] \sin(\mathbf{q}\mathbf{x}_s)$
Using this substitution the $Re[J(k,q)J(k,-q)]$ product becomes:

$$Re[J(k,q)J(k,-q)] =$$
$$Q_c^2\ Re\left[\left(\sum_s P_s Q_s^{(q)}\left[\mathcal{C}_s^{(q)} + i\,\mathcal{S}_s^{(q)}\right]\right) \times \left(\sum_{s'} P_s Q_{s'}^{(-q)}\left[\mathcal{C}_{s'}^{(-q)} + i\,\mathcal{S}_{s'}^{(-q)}\right]\right)\right] =$$
$$Q_c^2\ \left(\sum_s P_s^2\left[\mathcal{C}_s^{(q)}\mathcal{C}_s^{(-q)} - \mathcal{S}_s^{(q)}\mathcal{S}_s^{(-q)}\right] + 2\sum_{s>s'} P_s P_{s'} Q_s^{(q)} Q_{s'}^{(-q)}\left[\mathcal{C}_s^{(q)}\mathcal{C}_{s'}^{(-q)} - \mathcal{S}_s^{(q)}\mathcal{S}_{s'}^{(-q)}\right]\right) \tag{6.26}$$

Here we exploited the fact that in the product $J(k,q)\,J(k,-q)$ the factor $Q_s^q\,Q_s^{-q}$ reduces to unity.

Thus the correlation function becomes:

$$C(k,q) = 1 + \exp(-R^2q^2)\times \frac{\sum_s P_s^2\left[\mathcal{C}_s^{(q)}\mathcal{C}_s^{(-q)} - \mathcal{S}_s^{(q)}\mathcal{S}_s^{(-q)}\right] + 2\sum_{s>s'} P_s P_{s'} Q_s^{(q)} Q_{s'}^{(-q)}\left[\mathcal{C}_s^{(q)}\mathcal{C}_{s'}^{(-q)} - \mathcal{S}_s^{(q)}\mathcal{S}_{s'}^{(-q)}\right]}{\sum_s P_s^2\,\mathcal{K}_s^2 + 2\sum_{s>s'} P_s P_{s'}\mathcal{K}_s\mathcal{K}_{s'}} \tag{6.27}$$

For one pair of fluid cells this expression returned the correlations function expression given in Eq. 2.17.

The method presented in this appendix exploits the global symmetry of a Heavy Ion Collision across the c.m. point. This makes a factor of N_{cell}^2 reduction in the summation, although the expressions become slightly more complex. The formulae for the evaluation include double summations over cell-pairs denoted by "s", nevertheless, the correlations between any of the cells with any other cell are included in the summation.

Now we also have to evaluate the weight factor, w_s for the fluid cells in the hydro model, presented in Eq. (4.6).

This weight is is the same for all directions of $\mathbf{k}$, so also for the mirror image cells: $w_s^* = w_s$, if $\Theta_s^2(\mathbf{x}_s)$ is the same for both. Nevertheless, the factors

$\exp[\mathbf{ku}/T_s]$ in the $\mathcal{K}$, $\mathcal{C}_s^{(q)}$, and$\mathcal{S}_s^{(q)}$-functions will give strong dominance for the fluid cells, which move towards $\mathbf{k}$.

In the case when the weights for the cells and the mirror image cells are the same, $w_s^* = w_s$, thus the correlation function only includes cos and cosh terms, see Eq. 2.29. So, the *direction* of the velocity, $\mathbf{v}$, does not influence the correlation function, it depends only on the magnitude of the velocities. However, if the weights are not the same correlation function will contain sinh terms also, as the mirror cells may contribute differently. This is shown by Eq. 3.3.

Thus we choose the most frequently used choice is to have the FO layer along a constant proper time hyperboloid. In this case we can choose the time-like FO normal as $\hat{\sigma}_{s\mu} = (\gamma_s, \mathbf{u}_s)$. Then $(k_\mu \hat{\sigma}_s^\mu) = \gamma_s k_0 + \mathbf{ku}_s$. So the weight becomes

$$w_s = (\gamma_s k_0 + \mathbf{ku}_s)\ \exp(-\Theta^2 q_0^2/2)\ . \tag{6.28}$$

This weight is explicitly different for the cell and its mirror image cell

$$w_s^* = (\gamma_s k_0 - \mathbf{ku}_s)\ \exp(-\Theta^2 q_0^2/2)\ . \tag{6.29}$$

This makes the correlation function asymmetric and sensitive to the direction of the rotation of the flow.

Even more sophisticated parametrizations are discussed in Refs. [18, 19].

Bibliography

[1] L.P. Csernai, V.K. Magas, H. Stöcker, and D.D. Strottman, Phys. Rev. C 84, 02914 (2011).

[2] L.P. Csernai, D.D. Strottman and Cs. Anderlik, Phys. Rev. C 85, 054901 (2012).

[3] D.J. Wang, Z. Néda, and L.P. Csernai Phys. Rev. C **87**, 024908 (2013).

[4] L.P. Csernai, V.K. Magas, and D.J. Wang, Phys. Rev. C (2013) in press.

[5] R. Hanbury Brown and R.Q. Twiss, Phil. Mag. **45** (1954) 663-682; and R. Hanbury Brown and R.Q. Twiss, Nature, **178** (1956) 1046-1048.

[6] G. Goldhaber, S. Goldhaber, W. Lee and A. Pais, Phys. Rev. **120** (1960) 300.

[7] D. Miskowiec, and E877 Collaboration, Nucl. Phys. A **590**, 557c (1995).

[8] M.A. Lisa, N.N. Ajitanand, J.M. Alexander, et al., Phys. Lett. B **496** (2000) 1; M.A. Lisa, U. Heinz, U.A. Wiedemann, Phys. Lett. B **489** (2000) 287.

[9] S. Pratt, Phys. Lett. B301 (1993) 795; S. Pratt and V. Zelevinsky, Phys. Rev. Lett. 72 (1994) 816.

[10] Yu.M. Sinyukov, Nucl. Phys. A498 (1989) 151c.

[11] Qingfeng Li, J. Steinheimer, H. Petersen, M. Bleicher, H. Stöcker, Phys. Lett. B **674**, 111 (2009); Qingfeng Li, M. Bleicher, H. Stöcker, Phys. Lett. B **659** 525 (2008); Qingfeng Li, M. Bleicher, Xianglei Zhu, H. Stöecker, J. Phys. G **33** 537 (2007).

[12] M.A. Lisa, S. Pratt, R. Soltz, U. Wiedemann, Annual Review of Nuclear and Particle Science, **55**, 357 (2005).

[13] Sz. Horvat, V.K. Magas, D.D. Strottman, L.P. Csernai, Phys. Lett. B 692, 277 (2010).

[14] L.P. Csernai: *Introduction to relativistic heavy ion collisions*, Wiley, Chichester, (1994)

[15] F. Cooper, G. Frye, Phys. Rev. D 10, 186 (1974)

[16] Cheuk-Yin Wong: *Introduction to heavy ion reactions*, World Scientific Publishing Co., Singapore (1994)

[17] W. Florkowski: *Phenomenology of Ultra-relativistic heavy-Ion Collisions*, World Scientific Publishing Co., Singapore (2010)

[18] E. Molnar, L. P. Csernai, V. K. Magas, Zs. I. Lazar, A. Nyiri, and K. Tamosiunas, *J. Phys.* **G 34** (2007) 1901-1916; arXiv: (nucl-th/0503048)

[19] E. Molnar, L. P. Csernai, V. K. Magas, A. Nyiri, and K. Tamosiunas, *Phys. Rev.* **C 74** (2006) 024907; arXiv: (nucl-th/0503047)

[20] E. Molnár, L.P. Csernai, V.K. Magas, *Acta Phys. Hung.* **A 27** (2006) 359. arXiv:(nucl-th/0510062)

[21] T. Csörgő, Heavy Ion Phys. 15, 1-80, (2002); arXiv:hep-ph/0001233v3

[22] D. Anchisken, V. Vovchenko, L.P. Csernai, in preparation (2012)

[23] A.N. Makhlin, Yu.M. Sinyukov, Z. Phys. C 39, 69-73 (1988)

[24] I.S. Gradshteyn and I.M. Ryzhik: *Table of integrals, series and products*, Academic Press (1965)

[25] P.K. Kovtun, D.T. Son and A.O. Starinets, Phys. Rev. Lett. 94, 111601 (2005).

[26] L.P. Csernai, J.I. Kapusta, L.D. McLerran, Phys. Rev. Lett. 97, 152303–4 (2006).

[27] L.P. Csernai, G. Eyyubova, V.K. Magas, Phys. Rev. C 86, 024912 (2012).

[28] Yu.M. Sinyukov, Yad. Fiz. 50, 228 (1989) Sov. J. Nucl. Phys. 50, 143 (1989); Z. Phys. C 43, 401 (1989).

[29] K.A. Bugaev, Nucl. Phys. A606, 559 (1996).

[30] Cs. Anderlik, Z.I. Lázár, V.K. Magas, L.P. Csernai, H. Stöcker and W. Greiner, *Phys. Rev.* **C59** (1999) 388.

[31] Cs. Anderlik, L.P. Csernai, F. Grassi, W. Greiner Y. Hama, T. Kodama, Zs. Lázár, V. Magas and H. Stöcker, *Phys. Rev.* **C59** (1999) 3309.

[32] V.K. Magas, Cs. Anderlik, L.P. Csernai, F. Grassi, W. Greiner Y. Hama, T. Kodama, Zs. Lázár and H. Stöcker, *Nucl. Phys.* **A661** (1999) 596c-599c.

[33] L.P. Csernai, *J. Phys.* **G28** (2002) 1993.

[34] V.K. Magas, A. Anderlik, Cs. Anderlik and L.P. Csernai, *Eur. Phys. J.* **C30** (2003) 255-261.

[35] K. Tamosiunas and L.P. Csernai, *Eur. Phys. J.* **A20** (2004) 269-275.

[36] V.K. Magas, L.P. Csernai, E. Molnár, A. Nyiri and K. Tamosiunas, *Nucl. Phys.* **A 749** (2005) 202-205.

[37] V.K. Magas, L.P. Csernai, E. Molnár, *Acta Phys. Hung.* **A 27** (2006) 351,; arXiv: nucl-th/0510066

[38] Stefan Floerchinger and Urs Achim Wiedemann, Journal of High Energy Physics, doi:10.1007/JHEP 11, 100 (2011); and J. Phys. G: Nucl. Part. Phys. 38, 124171 (2011).

[39] D. Anchishkin, V. Vovchenko, and L.P. Csernai, Phys. Rev. C **87**, 104906 (2013).

[40] V. Vovchenko, D. Anchishkin, and L.P. Csernai, in preparation.

[41] Y. Cheng, L.P. Csernai, V.K. Magas, B.R. Schlei, and D. Strottman, Phys. Rev. C **81**, 064910 (2010).

[42] P. Huovinen, H. Petersen, Eur. Phys. J. A **48**, 171 (2012)

[43] D. Anchishkin, V. Vovchenko, and S. Yezhov, Eur. Phys. J. A, in press.

[44] L.P. Csernai and D. Röhrich, Phys. Lett. **B 458** (1999) 454.

[45] J. Brachmann, A. Dumitru, H. Stöcker, W. Greiner, Phys. Rev. C **61**, 024909 (2000).